

INSTRUMENTATION FOR MODEL STUDIES
OF THE TWO-HORIZONTAL-COPLANAR-COIL METHOD OF
ELECTROMAGNETIC EXPLORATION

By

Lathrop VB. Denslow

ProQuest Number: 10795561

All rights reserved

INFORMATION TO ALL USERS

The quality of this reproduction is dependent upon the quality of the copy submitted.

In the unlikely event that the author did not send a complete manuscript and there are missing pages, these will be noted. Also, if material had to be removed, a note will indicate the deletion.



ProQuest 10795561


Published by ProQuest LLC (2018). Copyright of the Dissertation is held by the Author.

All rights reserved.

This work is protected against unauthorized copying under Title 17, United States Code
Microform Edition © ProQuest LLC.

ProQuest LLC.
789 East Eisenhower Parkway
P.O. Box 1346
Ann Arbor, MI 48106 – 1346

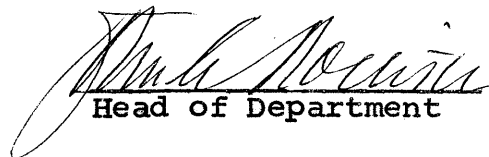
A Thesis submitted to the Faculty and the Board of Trustees of the Colorado School of Mines in partial fulfillment of the requirements for the degree of Master of Science in Geophysical Engineering.

Signed: 
Lathrop VB. Denslow

Golden, Colorado

Date: August 1, 1960

Approved: 
Thesis Advisor


Head of Department

Golden, Colorado

Date: 3 August, 1960

ABSTRACT

Model studies provide a practical method for the interpretation of electromagnetic exploration data. If displacement currents are neglected, which is shown to be valid under the most pessimistic exploration conditions, Maxwell's equations yield the similitude relationship

$$\sigma f (s)^2 = \sigma' f' (s')^2$$

where σ , f , and s are conductivity, frequency and an arbitrary length, respectively; unprimed and primed symbols denote field and model conditions, respectively.

Based on this equation, instrumentation is developed to model the widely used two-horizontal-coplanar-coil exploration method. An a-c comparator measures the in-phase and quadrature components of a secondary alternating magnetic field, arising from induced currents in an ore-model, in terms of the primary magnetic field of the source-coil.

Experimental data taken over a mercury sphere were compared with March's theoretical solution for the magnetic field of an oscillating magnetic dipole in the presence of a conducting sphere. Based on the conductivity of pure mercury, the experimental in-phase and quadrature secondary field components differ from theory by +31% and -1.4%, respectively. This discrepancy may be due to impurities in the mercury which have increased its conductivity.

Measurement of the actual conductivity of the mercury used, critical study of the limitations of the theoretical solution, reduction of the dimensions of the source- and receiver-coils, and derivation of the reference signal inductively from the transmission line to the source-coil, rather than from a reference coil wound on the source-coil, might lead to better correlation between experimental and theoretical response to a conducting sphere.

CONTENTS

Abstract.	iii
Acknowledgements.	viii
Introduction.	1
Model Theory.	5
Justification for Neglecting Displacement Currents	6
Derivation of Similtude Equation	7
Instrumentation	13
Framework.	13
Signal Source.	15
Coils.	18
A-C Comparator	21
Reference Circuit.	26
Null-Detector.	30
Verification of Instrumentation	35
Conclusions	47
Alternative Approaches	47
Significant Observations	53
Suggested Improvements	55
Appendices.	57
Appendix 1 - Preparation for Taking Data	57
Appendix 2 - Taking and Reducing Data.	60
Appendix 3 - A-C Comparator Calibration.	61
Appendix 4 - Extension of March's Solution for the Case of Finite Sphere Conductivity.	63
Selected Bibliography	66

ILLUSTRATIONS AND TABLE

Figure 1	Full-scale and model coordinate systems	9
Figure 2	Block-diagram of instrumentation.14
Figure 3	Signal-Source Components.16
Figure 4	Phase diagram for representing in-phase and quadrature components of secondary field23
Figure 5	A-C comparator circuit and phase diagram.25
Figure 6	Reference circuit and phase diagram29
Figure 7	Block-diagram of null-detector components31
Figure 8	Transistorized preamplifier circuit diagram32
Figure 9	High-gain narrow-band amplifier circuit diagram33
Figure 10	Spherical coordinates of March's sphere solution.36
Figure 11	Modeling dimensions and parameters in $\phi = 0$ plane of March's coordinate system.36
Figure 12	Experimental and theoretical anomalies over 500 ml mercury sphere - $d = 0.500$ ft.43
Figure 13	Experimental and theoretical anomalies over 500 ml mercury sphere - $d = 0.333$ ft.44
Figure 14	Circuit and phase diagrams for measuring magnitude and phase of secondary field.48
Figure 15	Circuit and phase diagrams for Ronka method of measuring in-phase and quadrature components of secondary field.50
Figure 16	Circuit diagram for "bucking coil" method of measuring in-phase and quadrature components of secondary field.52

Plate 1	Signal-source components.17
Plate 2	Source-coil, receiver-coil, and reference-coil over 500 ml mercury sphere17
Plate 3	A-C comparator and reference circuit chassis.27
Plate 4	A-C comparator and reference circuit together with null-detector components27
Table 1	Source-coil and receiver-coil specifications.19

ACKNOWLEDGEMENTS

I thank Dr. George T. Merideth of the Colorado School of Mines for his valuable advice and counsel both during the development of the modeling equipment and while writing the thesis. I am grateful also to Profs. Frank Mathews and Albert Gosman for their constructive suggestions and criticisms.

The Bear Creek Mining Company of Denver has been very generous in providing space, equipment, facilities, and financial support during the development of this thesis. George Rogers and Jim Harrison have been particularly helpful.

Special thanks is due to the National Science Foundation for providing a fellowship under which the early stages of this thesis was conducted.

Finally, I shall always be in debt to my friend, Bill Stockwell, who voluntarily spent many long hours assisting me in constructing and testing the modeling system.

INTRODUCTION

Inductive electromagnetic exploration methods provide a powerful tool for the discovery of conducting ore-bodies. Since the early 1920's numerous variations in method have been tried with varying degrees of success. Some methods work well under certain geologic conditions and poorly in others; some are better suited for reconnaissance than for detail surveying.

With the exception of the audio-frequency magnetometer (AFMAG) system presently being developed, all inductive electromagnetic exploration methods involve a man-made source of alternating magnetic field and a receiver which senses the field. The source and receiver, which usually consist of planar coils of wire, are inductively coupled with the ground and with each other.

The alternating magnetic field of the source-coil (primary field) induces currents in subsurface conductors. These currents constitute the source of a second alternating magnetic field (secondary field) which combines vectorially with the primary field to produce a net or total alternating

magnetic field. Because of the resistance and inductance of subsurface conductors, the secondary field generally has components in-phase and at quadrature with the primary field. The receiving-coil senses the space component of the total field in the direction of its axis. It is from the measurements of certain diagnostic aspects of the total field that geophysicists hope to determine the nature of the conductors which give rise to the secondary field.

Abstractly, we can think of this process as the interaction of two sets of independent variables, one known and one unknown, to produce a field. By examining this field and accounting for the set of known variables, we try to deduce the nature of the set of unknown variables. This last step, interpretation, has been highly dependent for success on the experience, skill, and imagination of the interpreter.

In seismic, gravity, and magnetic prospecting, theory has been of great value in developing useful interpretation techniques. Electromagnetic theory, however, because of the highly complex mathematics involved, has yielded only a few solutions. These solutions are of rather limited value in interpreting electromagnetic field data because they deal with only the simplest conditions of geometry and conductivity. In contrast, theory has shown that electromagnetic exploration systems can be accurately

modeled on a scale suitable for laboratory studies so that the results obtained can be directly applied to interpreting field data. This approach, long used in Sweden, is now becoming widely recognized in North America as a practical means of obtaining quantitative interpretations of electromagnetic field data.

Past experience has shown that it is not necessary to measure completely the direction, intensity, and phase at the receiver location in order to obtain sufficient information on which to base an interpretation. One method measures only the dip of the field at several points about a fixed source; another method measures only the quadrature component of a horizontal component of the alternating magnetic field as the source and receiver together move over a traverse.

Still another method, one which is widely used in the United States, Canada, and Scandinavia, is described as the two-horizontal-coplanar-coil method. The two coils are kept at a fixed separation and moved over a traverse. The source-coil sets up an oscillating vertical magnetic dipole. From the receiver signal, the in-phase and quadrature components of the vertical component of the secondary field are measured relative to the primary field. These two measurements, when taken at a number of points

along a traverse, theoretically contain positive quantitative information about depth, size, shape, orientation, and conductivity of subsurface conductors. The real extent and limitations of this method have yet to be determined through extensive model studies.

In view of the great potential value of the modeling technique in providing a practical method of interpretation, and the widespread use of the above-described exploration method, it is the objective of this thesis to design, construct, and verify a laboratory system for making model studies of the two-horizontal-coplanar-coil method. The equipment developed for this thesis can readily be modified to model other coil arrangements involving similar phase measurements.

MODEL THEORY

The theory of electromagnetic models is presented with rigor and detail in several texts, papers and related theses. The treatments by Sinclair (1948, p. 1364-1370) and the extensions by Ward (1953, p. 9-12, 38-48), from both of whom I draw in the discussions to follow, constitute an excellent fundamental development of the similitude equations. The pattern of their combined development is to derive, from Maxwell's electromagnetic equations, the requirements for an absolute model (i.e., a model in which power levels as well as field configurations are simulated). These requirements are then reduced to the case of a geometric model (i.e., a model in which only the field configuration is modeled). Finally the requirements are further reduced to the case of a geometric model in which the displacement current can be neglected. This last case is the one of interest in this study since only relative field measurements are made. For the reader's convenience I shall justify neglecting displacement

currents for ordinary electromagnetic prospecting, and then present a short development of the appropriate similitude equation.

Justification for Neglecting Displacement Currents

From Maxwell's equation for steady state, current density, \underline{J} , may be written as the sum of conduction and displacement currents.

$$\underline{J} = \sigma \left(1 + i \frac{\omega \epsilon}{\sigma} \right) \underline{E}$$

Where σ is conductivity, ω is angular frequency, ϵ is permittivity, \underline{E} is a sinusoidal electric field, and i denotes $(-1)^{1/2}$. If $\frac{\omega \epsilon}{\sigma} \ll 1$, then displacement currents are negligible. The conductivities of most massive sulfides fall within the range 10^{-1} to 10^4 mhos/m. Natural dielectric constants, K_ϵ , vary from 1 to about 80. Since $\epsilon = K_\epsilon \epsilon_0$ where $\epsilon_0 = 8.85 \times 10^{-12}$ farad/m is the permittivity of free space, the range of ϵ is from about 9×10^{-12} to about 700×10^{-12} farad/m. With a maximum useful field frequency of 10 kc, the maximum ω is 62.8×10^3 /sec. Therefore $\frac{\omega \epsilon}{\sigma}$ has a maximum value of 0.00045; this demonstrates that for the most pessimistic case, the displacement currents arising in ore-bodies subjected to electromagnetic exploration methods are very much less than conductive currents, and can justly be neglected.

Derivation of Similitude Equation

To derive the electromagnetic similitude equation for the case of a geometric model when displacement currents can be neglected, let us consider the point $P(x,y,z)$ of the full scale system, as shown in figure 1, and the corresponding point $P'(x', y', z')$ of the model system. Let p be the mechanical scale factor between the full-scale and model coordinates so that the coordinate transformations are

$$x = px' \quad (1a)$$

$$y = py' \quad (1b)$$

$$z = pz' \quad (1c)$$

In addition, let the scale factors for time, t , electric field, \underline{E} , and magnetic field, \underline{H} , be defined by

$$t = \gamma t' \quad (2)$$

$$\underline{E} = \alpha \underline{E}' \quad (3)$$

$$\underline{H} = \beta \underline{H}' \quad (4)$$

Omitting displacement currents, Maxwell's equations for the full-scale system are

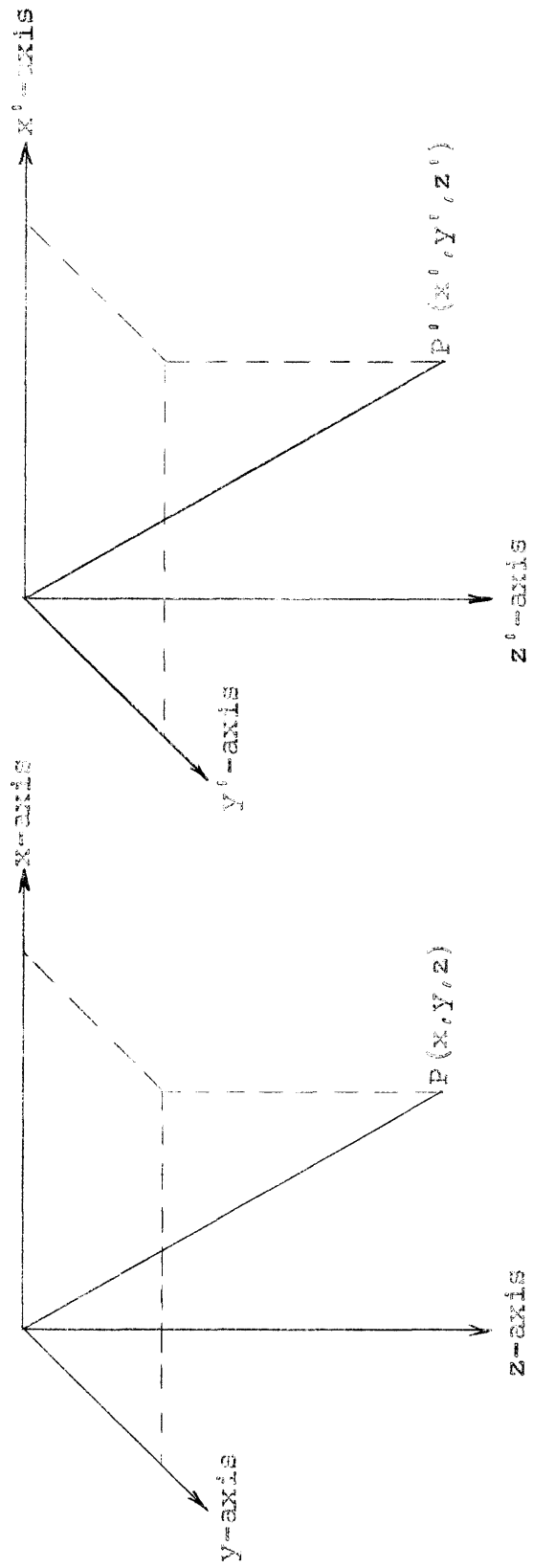


Figure 1 - Full-scale and model coordinate systems

$$\underline{\nabla} \times \underline{E} = -\mu \frac{\partial}{\partial t} \underline{H} \quad (5)$$

$$\underline{\nabla} \times \underline{H} = \sigma \underline{E} \quad (6)$$

where μ is permeability and σ is conductivity. The corresponding equations for the model are

$$\underline{\nabla}' \times \underline{E}' = -\mu' \frac{\partial}{\partial t'} \underline{H}' \quad (7)$$

$$\underline{\nabla}' \times \underline{H}' = \sigma' \underline{E}' \quad (8)$$

where $\underline{\nabla}'$ implies taking derivatives with respect to the primed coordinates. If the model is an accurate simulation of the full-scale system, then substituting the transformations (1) to (4) into (7) and (8) should yield equations (5) and (6). Employing the transformations, (7) and (8) become

$$\frac{\rho}{\alpha} \underline{\nabla} \times \underline{E} = -\mu' \frac{\gamma}{\beta} \frac{\partial}{\partial t} \underline{H} \quad (9)$$

$$\frac{\rho}{\beta} \underline{\nabla} \times \underline{H} = \sigma' \frac{1}{\alpha} \underline{E} \quad (10)$$

Since these must be identical with (5) and (6), we have

$$\mu = \frac{\alpha \gamma}{\beta \rho} \quad (11)$$

$$\sigma = \frac{\beta}{\alpha \rho} \sigma' \quad (12)$$

which constitute the only theoretical restrictions on the

four scale factors, α , β , γ , and ρ . However, there is a practical restriction on μ . If ferromagnetic materials are to be avoided in modeling the free space of the full-scale system, then the permeability of all corresponding parts of both systems must be the same; this implies

$$\mu = \mu'. \quad (13)$$

It follows that

$$\frac{\alpha \gamma}{\beta \rho} = 1 \quad (14a)$$

or

$$\frac{\alpha}{\beta} = \frac{\rho}{\gamma}. \quad (14b)$$

Since ratios of magnetic fields rather than field magnitudes are to be measured with the instruments developed in this thesis, the values of α , β , and α/β are of no interest.

In order to put the above results into a simple form immediately useful for modeling electromagnetic prospecting systems, we consider the relationship between the three significant variables: length, frequency, and conductivity. Since the three orthogonal components of length are scaled by the same factor, then some arbitrary length, s , such as coil separation, is scaled by that

factor also.

$$s = ps' \quad (15)$$

Since frequency, f , is inversely proportional to time,

$$f = \frac{1}{\gamma} f' \quad (16)$$

Substituting (14b) into (12), we find that

$$\sigma = \frac{\gamma}{p^2} \sigma' \quad (17)$$

Now, since γ and p can be varied independently, the above model requirements can be written as the single relationship

$$\sigma f (s)^2 = \sigma' f' (s')^2 \quad (18)$$

This simple equation gives the experimenter great freedom in modeling a given field situation. There is a wide range of values of σ' , f' , and s' from which he may choose a combination for his studies. Conversely, a single model experiment will apply equally well to a whole range of field conditions. Frequently it is convenient to use the same frequency in a model study as that used in the field. In this case all length dimensions are decreased by the factor p in order to be modeled, and the conductivity is increased by the factor p^2 . It turns out that if such an arrangement is used, the value of $p = 200$, often a

convenient scale factor, requires a modeling material with a conductivity 4×10^4 times larger than the field conductivity. Thus the massive sulfide conductivity range of 10^{-1} to 10^4 mhos/m must be modeled by materials in the conductivity range 4×10^3 to 4×10^8 mhos/m. The conductivities of carbon, graphite and the common metals cover most of this range, thus permitting ready modeling of massive sulfide conductivities.

INSTRUMENTATION

Any system for conducting electromagnetic model studies must contain several basic components: a framework to permit desired orientations of the source-coil, the receiver-coil, and the simulated ore-body, a signal source, a receiver, and circuitry to extract the desired information from the receiver signal. The various components of the instrumentation developed for this thesis will be discussed below. The electrical portion of the instrumentation will be discussed in the sections indicated in the block diagram of figure 2. The procedures for preparing the system for running a traverse, and for taking and reducing data are given in Appendices 1 and 2, respectively.

Framework

The framework about which I built the electrical portion of the system was available at the Bear Creek Mining Company from a previous modeling set-up. It is rectangular

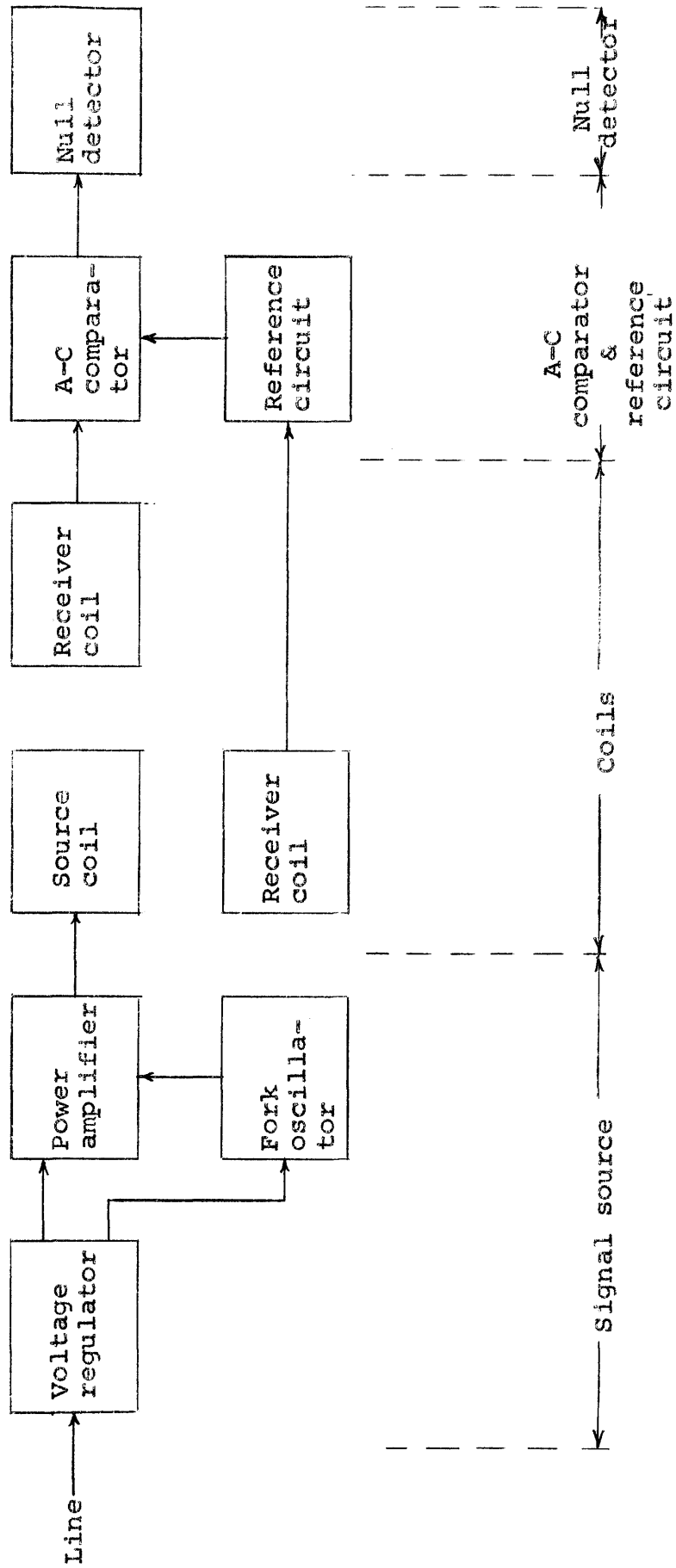


Figure 2 - Block diagram of instrumentation

and very rigidly constructed of heavy mahogany beams. It includes a nonconducting carriage to support the coils, adjust their vertical location, and move them in a horizontal traverse over a simulated ore-body. The ore-model is held by a nonconducting secondary frame which rests on the floor. The coordinate framework contains no metal parts and has built-in scales which permit successive positioning of the coils to an accuracy of about 0.005 foot.

Signal Source

Figure 3 shows a detailed diagram of the signal source components except for the source-coil which will be discussed in the next section. Plate 1 is a photograph of the same components. The Riverbank 1000-cps fork oscillator was used after discovering that frequency drift of the Hewlett Packard Model 650A oscillator originally used was sufficient to cause a significant shift in the null position of the a-c comparator over an interval of only a few minutes. Since the 53-volt output of the fork oscillator was much too large to drive the power amplifier, a shielded attenuation circuit was inserted as shown in figure 3. Shielding was provided in an attempt to reduce stray 60-cps input to the power amplifier. The attenuation

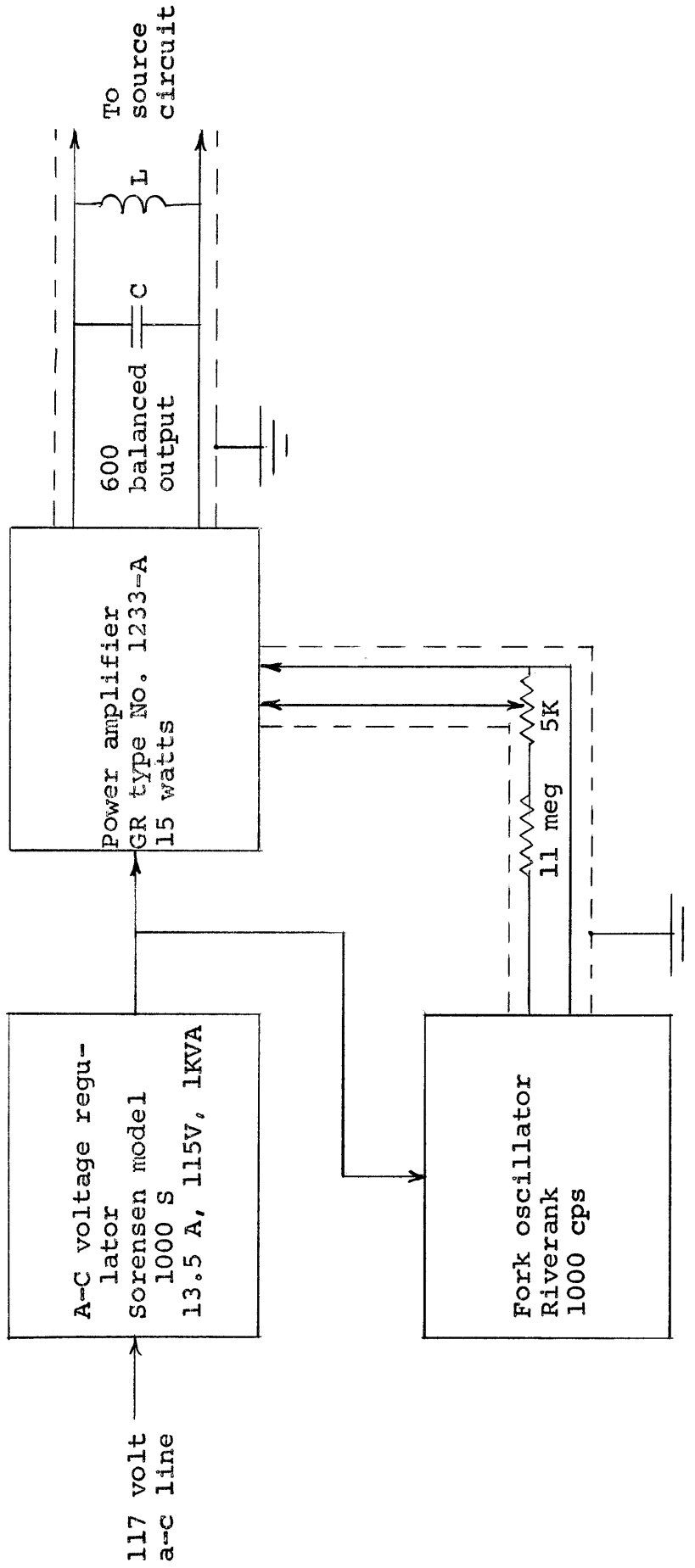


Figure 3 - Signal-source components

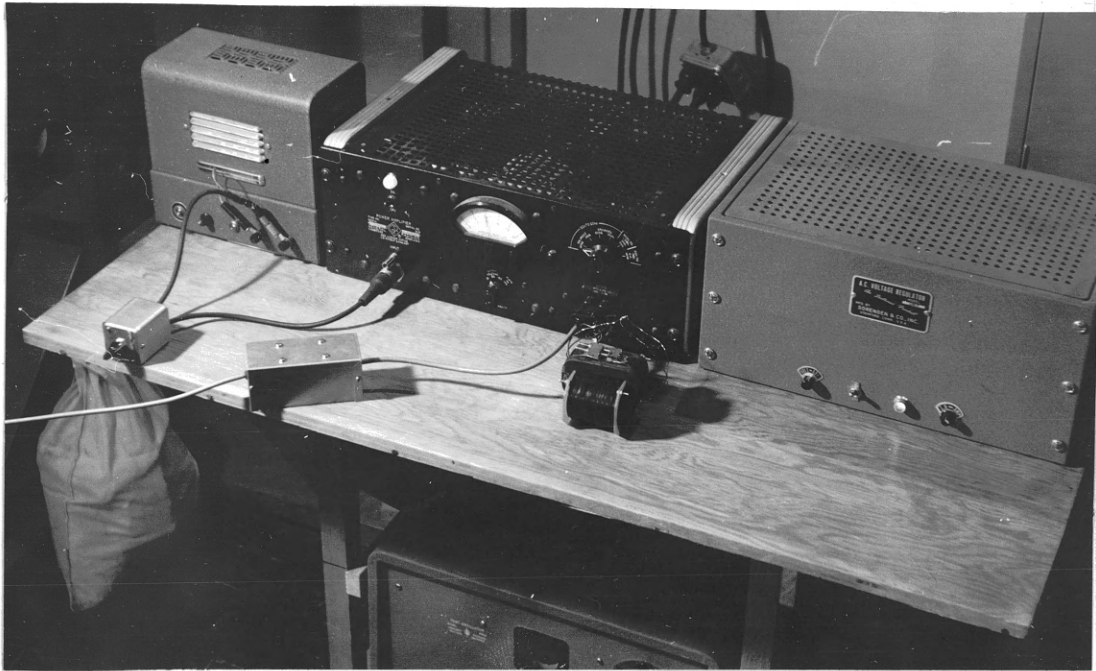


Plate 1 - Signal-source components



Plate 2 - Source-coil, receiver-coil, and reference-coil over 500 ml mercury sphere

circuit provides a signal variable from 0 to 25 mv, which corresponds to an output of 0 to 29 v from the power amplifier when loaded with 600 ohms.

Because of some distortion and 60-cps noise appearing in the balanced 600-ohm output of the power amplifier, the output was shunted with a low-resistance tank circuit. This circuit resulted in a very clean sinusoidal output waveform. The 15-watt output of the amplifier is well in excess of that required. At 20-volts output the source-coil draws less than 1-watt.

Coils

Because of space limitations and particular model studies to be undertaken when the instrumentation was completed, it was decided to base the coil design on a coil spacing of one foot. In order to avoid quadrupole and higher multipole fields of significant strength from arising from the source-coil, and in order that the receiver-coil sense the average field over as small an area as practical, it was assumed that the diameters and lengths of the coils should be of the order of one-tenth the coil separation or less. Plate 2 shows the coils over a 500 ml mercury sphere, and table 1 shows the specifications of the source- and receiver-coils used.

TABLE 1

Source-Coil and Receiver-Coil Specifications

<u>Specifications</u>	<u>Source</u>	<u>Receiver</u>
Outside Diameter (in.)	1.40	1.25
Inside Diameter (in.)	0.80	0.75
Height (in.)	1.25	0.50
Wire: Diameter (in.)	0.006304	0.003145
Gage (AWG)	34	40
Insulation	enamel	enamel
No. of Turns (approx.)	8,000	11,000
D-C Resistance (ohms)	593	3,050
Inductance (henries)	3.24	2.13
Q (at 1000-cps)	33.5	3.22
Core: Material	ferrite	air
Diameter (in.)	0.75	--
Length (in.)	1.50	--

The source-coil circuit is series tuned at the power amplifier with two matched capacitors. Its tuned impedance is about 600-ohms resistance to match the output impedance of the power amplifier. Because of the high Q of the source-coil, an input voltage of about 20-volts is used, resulting in about 600-volts across the coil and 300-volts across each tuning capacitor. It was found that an input voltage in excess of 50-volts caused insulation breakdown of the coil lead going to the inner windings, and internal shorting of the mica tuning capacitors. Two-conductor shielded cable connects the tuning capacitors at the power amplifier to the source-coil. The shield is grounded at the amplifier.

The receiver-coil is connected by two-conductor shielded cable to the a-c comparator, with the shield grounded at the comparator. It was not necessary to shield either the source- or receiver-coil. These coils are mounted on a bakelite beam in such a manner that their central planes are coplanar.

A reference-coil of 30 turns of number 28 AWG wire is wound in two symmetrical parts directly on the source-coil; it is center-tapped to the shield of the two-conductor cable which connects the reference-coil to the reference circuit. The shield is grounded at the reference circuit,

and the center-tap location adjusted to provide the necessary balanced reference signal.

A-C Comparator

The a-c comparator might well be called the heart of the modeling instrumentation. As mentioned in the Introduction, its function is to measure the in-phase and quadrature components of the vertical component of the secondary magnetic field as fractions of the (vertical) primary field at the receiver-coil location. The primary field constitutes the in-phase reference.

From the steady-state Maxwell equation

$$\underline{\nabla} \times \underline{E} = -i\mu\omega \underline{H}$$

it is evident that, for a given frequency, the receiver-coil voltage has a magnitude proportional to the magnetic field component parallel to the coil's axis, and at a constant phase angle to that field. One method of making the desired measurements, a method used in several designs of field equipment, is to put the receiver in series with a second signal of the same frequency but variable magnitude and phase. By successive adjustments of the second source, the sum of the two signals can be brought to zero, at which point the second signal is equal in magnitude

and 180° out-of-phase with the receiver signal.

Given a reference signal with variable phase and magnitude, there are several ways the second signal might be produced. However, since it is desired to know the receiver signal in terms of in-phase and quadrature components, it is desirable to design the source of the second signal to read these values directly. A simple way to do this is to produce quadrature voltages across two potentiometers. Figure 4 shows the desired phase diagram where $\underline{V}_{gi} \perp \underline{V}_{pq}$, $\underline{V}_{gz} = \underline{V}_{zi}$, $\underline{V}_{pi} = \underline{V}_{iq}$, and $|\underline{V}_{iq}| = 1/2 |\underline{V}_{zi}|$. \underline{V}_{gi} is the voltage across the in-phase potentiometer, and \underline{V}_{pq} across the quadrature potentiometer, the points z and i representing the respective mid-positions of the potentiometer sliders. The voltage between the two sliders constitutes the second signal. If the magnitude and phase of the voltage configuration of figure 4 are adjusted so that a null results when \underline{V}_{zi} is added to the primary receiver signal (no conducting body being present), then \underline{V}_{zi} corresponds to an in-phase reference which is 100% the magnitude of the primary receiver signal. With an ore-model in the vicinity of the coils, any deviations of the potentiometer sliders from their positions at z and i respectively, are a direct indication of the magnitude of the phase components

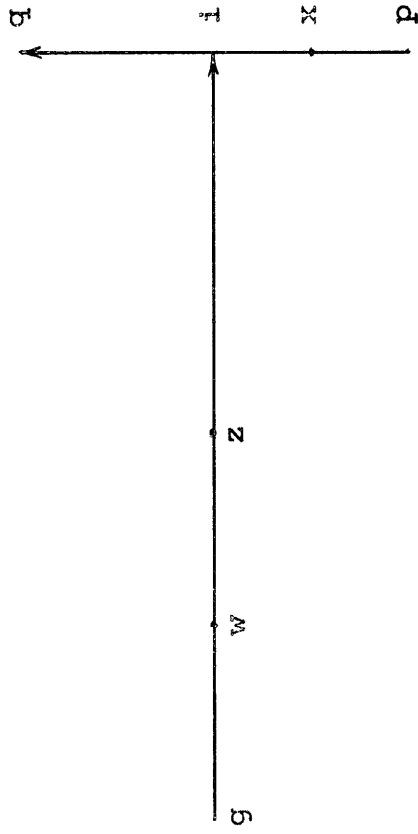


Figure 4 - Phase diagram for representing in-phase and quadrature components of secondary field

of the secondary field in terms of the magnitude of the primary field. Thus, if a null was achieved with the in-phase and quadrature sliders at w and x respectively (where $V_{wz} = (1/2)V_{zi}$, and $V_{xi} = (1/2)V_{pi}$), the secondary field components would be +50% in-phase and -25% quadrature. Any secondary field with an in-phase component between -100% and +100% and a quadrature component between -50% and +50% of the primary field can thus be directly measured.

The circuitry used to produce the phase diagram of figure 4 from a properly attenuated and phase-shifted reference signal is shown in figure 5. In order to produce the negative part of the quadrature voltage, V_{pi} , the circuit was built symmetrically about i. Figure 5 also shows the complete phase diagram.

An examination of the circuit diagram together with the phase diagram will show that the essence of the circuit lies in shunting R_1 with C_2 and R_2 in series to produce the vector triangle g-m-i of figure 5. Then by shunting R_2 with C_3 and R_3 in series, the vector triangle m-p-i is produced which includes the quadrature leg, p-i. The other half of the circuit is symmetrically identical. R_4 , the quadrature ten-turn potentiometer shunting R_3 and R_3' , permits continuous access to the quadrature voltage

To null detector

- $R_1 = 998 \Omega$
- $R_{1'} = 0 - 100 \Omega$
- $R_{1''} = 910 \Omega$
- $R_2, R_2' = 2026 \Omega$
- $R_3, R_3' = 544 \Omega$
- $R_4 = 4900 \Omega$
- $R_5 = 3900 \Omega$
- $R_{5'} = 0 - 1000 \Omega$
- $R_{5''} = 2700 \Omega$
- $R_6 = 3900 \Omega$
- $R_{6'} = 0 - 1000 \Omega$
- $C_1, C_1' = 0.022 \mu\text{f}$
- $C_2, C_2' = 0.240 \mu\text{f}$
- $C_3, C_3' = 0.245 \mu\text{f}$

$T_1 =$ Western Electric, input transf, model 618 D

From receiver coil

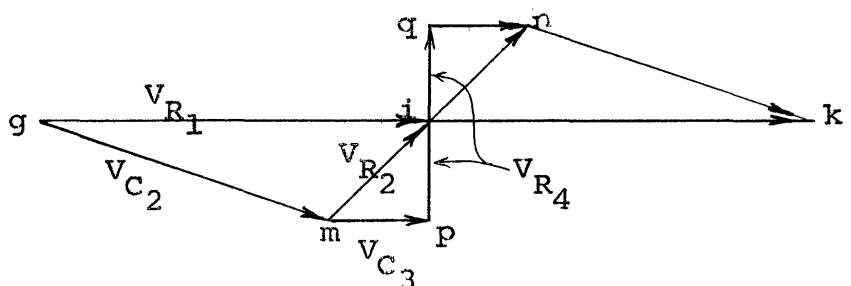
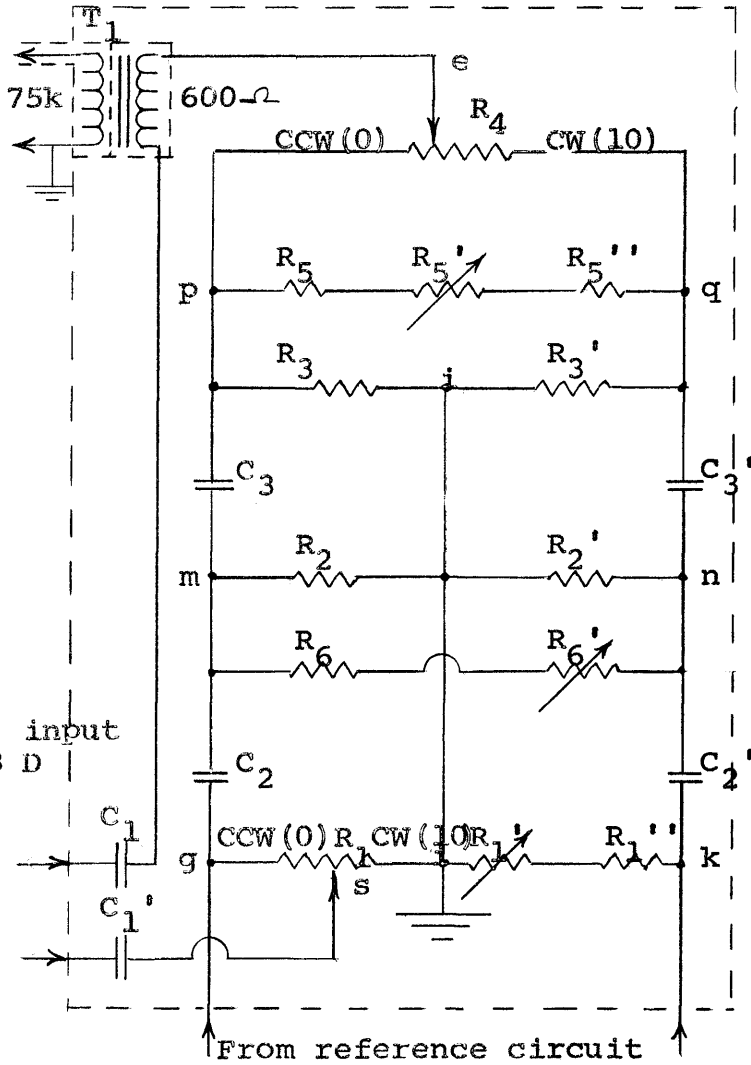


Figure 5 - A-C comparator circuit and phase diagram

distribution. R_5' and R_6' permit adjustment of the phase diagram to the desired form. R_1 , the in-phase ten-turn potentiometer, has continuous access to the in-phase voltage distribution.

The exact values of the circuit components are not important, but it is of major importance that symmetric components be closely matched. R_5' and R_6' can compensate for any component values which are only nominally those indicated in figure 5. All components used in constructing the comparator were matched with their symmetric counterparts to within 0.1%.

The circuit was constructed with as much physical symmetry as possible, and in order to balance any stray capacitances to the grounded chassis, the symmetric "point" of the circuit, i , was grounded. Plate 3 shows the a-c comparator chassis and its symmetric construction. The procedure for calibrating the comparator phase-relationship is given in Appendix 3.

Reference Circuit

The function of the reference circuit is to supply the a-c comparator with a balanced reference signal of the proper magnitude and phase such that the receiver signal, with no ore-model present, is nulled by the voltage V_{zi}

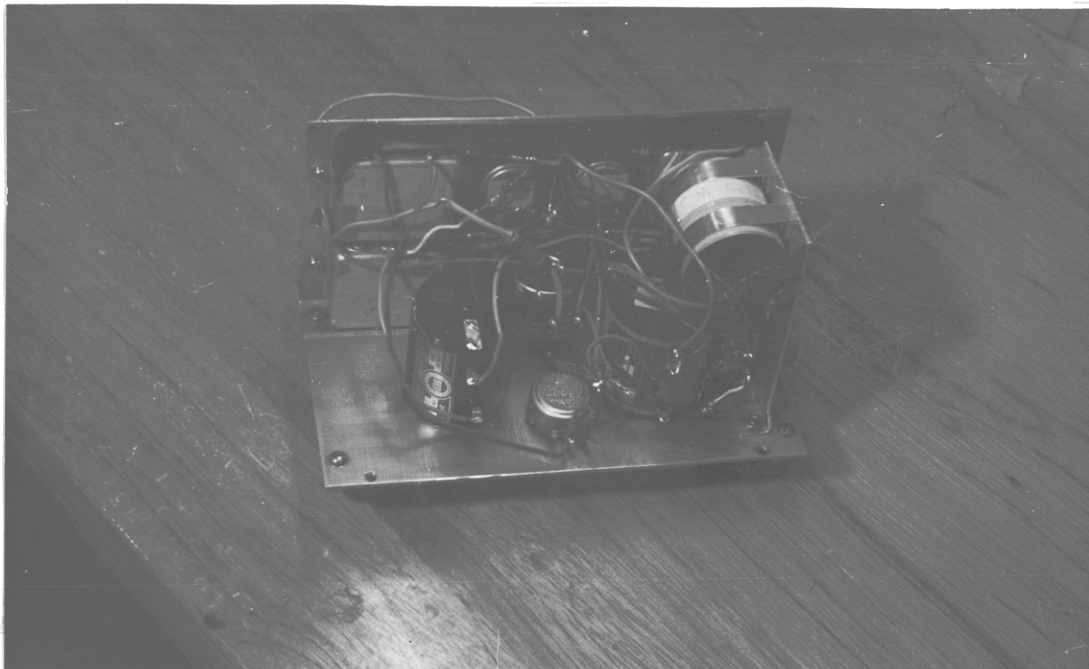


Plate 3 - A-C comparator and reference circuit chassis

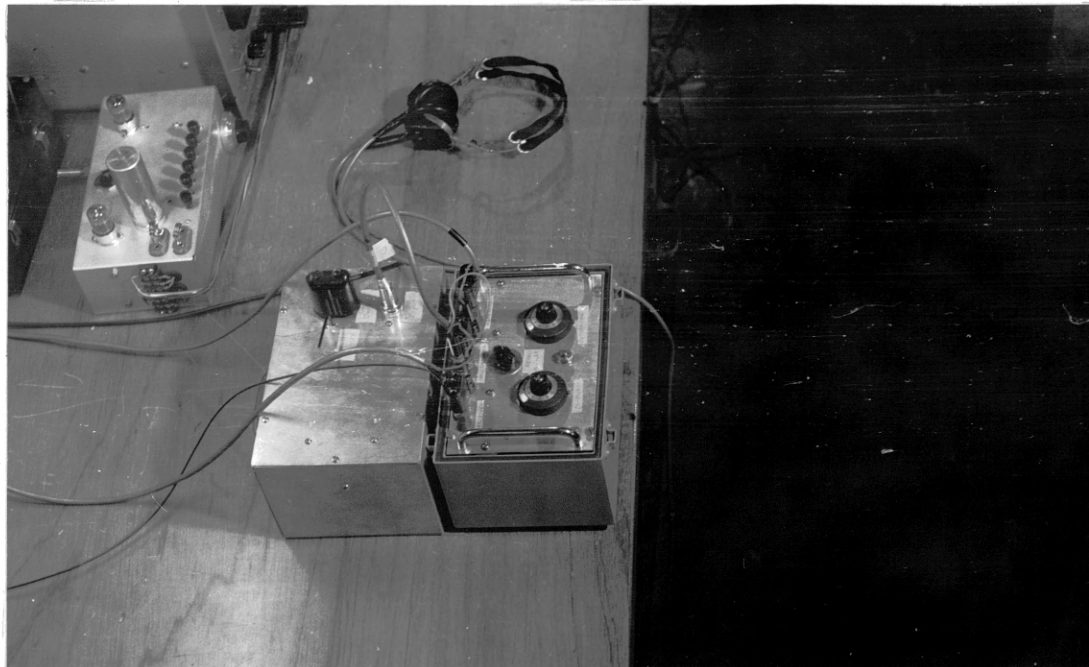
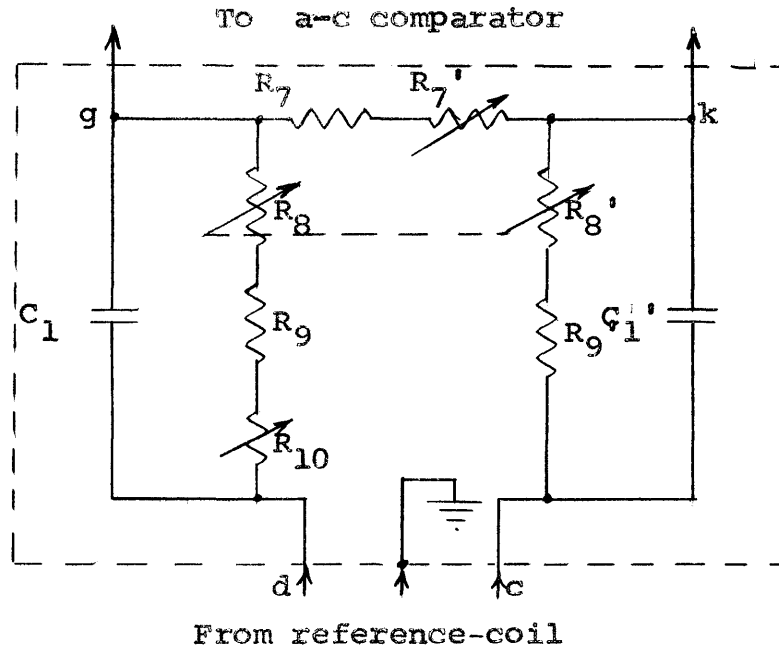


Plate 4 - A-C comparator and reference circuit
together with null-detector components

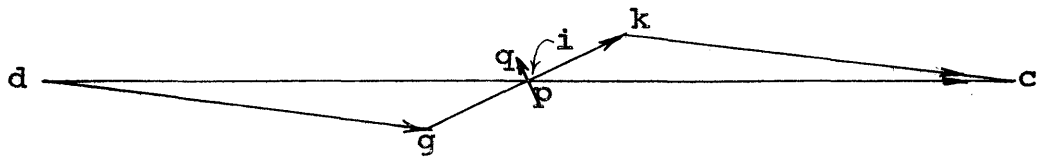
of figure 4. The reference-coil described above provides a balanced signal to the reference circuit. Because of the close coupling of the reference-coil with the source-coil, the reference-coil signal is essentially always proportional in magnitude to the primary field intensity, and has a constant phase relationship with the primary field.

The circuit shown in figure 6 serves to attenuate and phase shift the reference-coil signal in the desired manner. The idea behind this design is clear if we consider the circuit diagram together with the phase diagram of the same figure, and think of the a-c comparator as a partially capacitive impedance appearing between two matched, but variable, resistive-capacitive impedances, all three impedances being in series with the reference-coil signal. The phase and magnitude of the voltage across the a-c comparator may be altered by varying the tandem resistors R_8 and R_8' of the matched impedances. However, in order to control phase and magnitude independently, it is necessary to shunt the comparator with a variable resistance, R_7 . The a-c comparator and reference circuit are built into the same chassis. This unit is shown in Plate 4.

The component values shown in figure 6 were determined experimentally. C_1 and C_1' are matched to within 0.01%,



- $R_7 = 3.3k$
- $R_7' = 0 - 1000 \Omega$
- $R_8, R_8' = 0 - 300 \Omega$
- $R_9, R_9' = 4k$
- $R_{10} = 0 - 25 \Omega$
- $C_1, C_1' = 0.013 \mu f$



points q and p are shown in phase diagram of figure 5.

Figure 6 - Reference circuit and phase diagram

and R_{10} provides fine matching of the resistances R_8 and R_8' since they are not identical in their particular characteristics.

Null-Detector

The null-detector serves to amplify the output signal of the a-c comparator so that the in-phase and quadrature potentiometer settings required to balance any given receiver signal can be determined accurately. A detailed block-diagram of the null-detector circuit is shown in figure 7.

The two battery-powered amplifiers provide sufficient gain of the comparator output signal that headphones can be used to listen for a null. However, when the null is nearly achieved, stray 60-cps noise coming from the comparator becomes an appreciable part of the signal, thereby making exact nulling difficult. Therefore, the high-gain narrow-band amplifier with variable feedback, is inserted in the nulling circuit. This circuit addition permits adjustment of the null to a precision of about 0.05% of the primary field when feedback is adjusted almost to the point of oscillation. The circuit diagrams of the preamplifier and high-gain narrow-band amplifier are shown in figures 8 and 9. Plate 4 shows the components of the

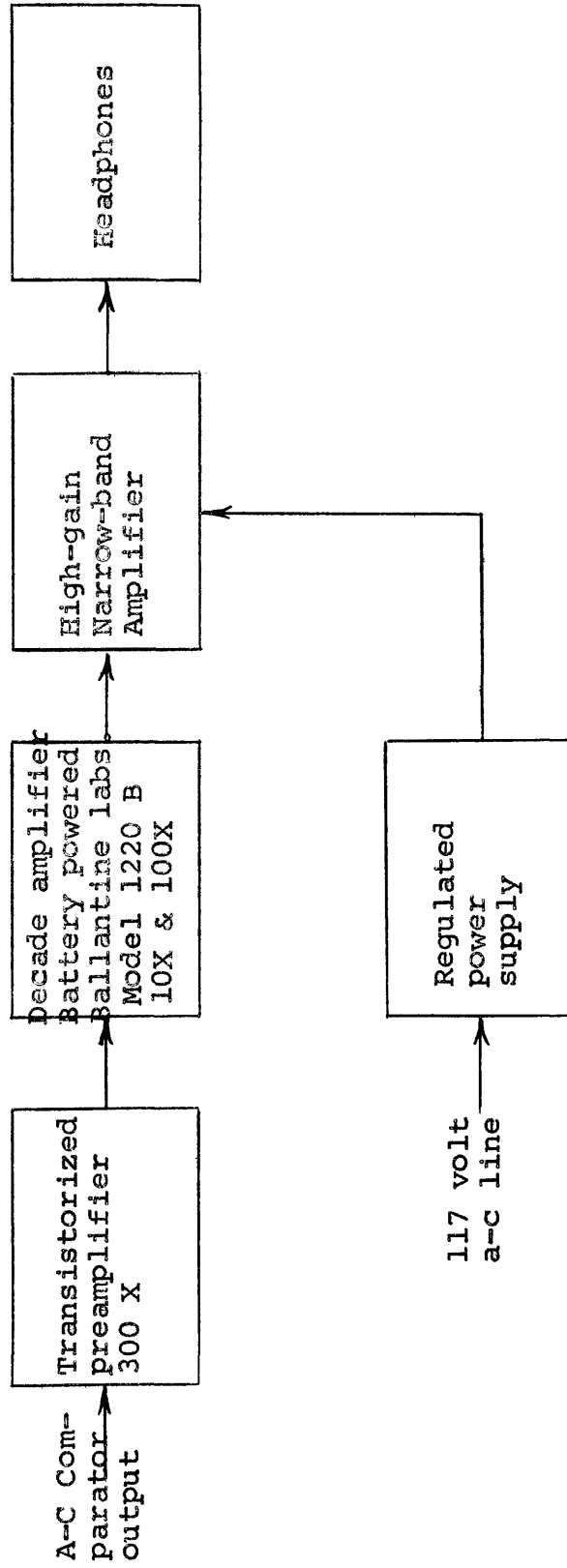


Figure 7 - Block-diagram of null-detector components

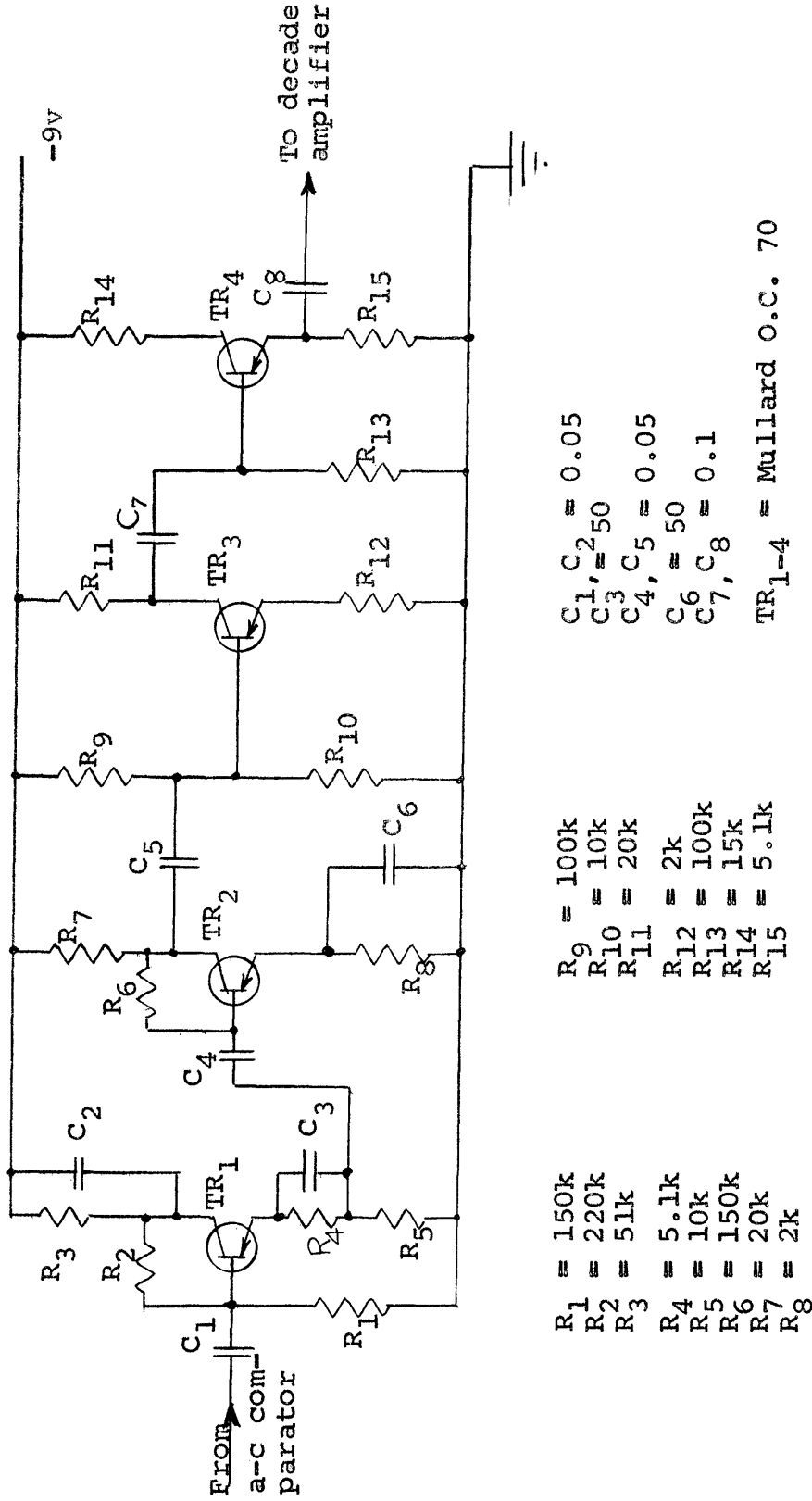


Figure 8 - Transistorized preamplifier circuit diagram.

Taken from Waters and Francis (1958, p. 91)

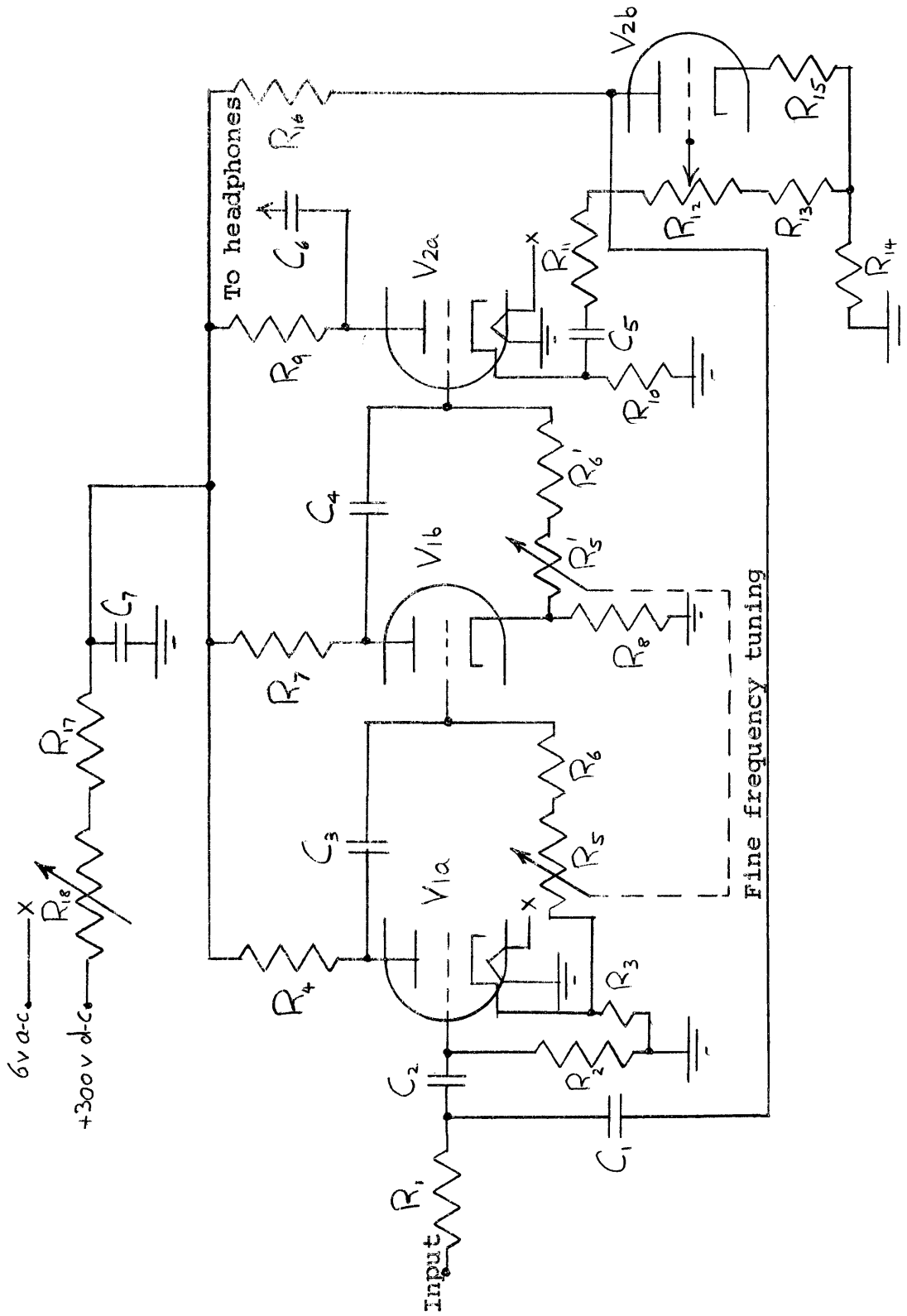


Figure 9 - High-gain narrow-band amplifier circuit diagram.
 Circuit available through Geophysics Dept., CSM

null-detector circuit and their physical arrangement
with the a-c comparator and reference circuit chassis.

VERIFICATION OF INSTRUMENTATION

The validity of the modeling system developed in this thesis is tested by comparing experimental anomalies with theoretical solutions. Of the very few boundary-value problems which have been solved for conducting bodies in an oscillating magnetic dipole field, the sphere solution of March (1953, p. 671-684) is one more readily reduced to a form which can be compared with experimental results.

The formulas derived by March are approximate and restricted to the special case in which conductivity is low, the radius of the sphere is small relative to wave length, and the source-dipole and observer are in the vicinity of the sphere. The case of spherical ore-bodies buried in a mass of rock is included within these restrictions. From model theory, the case of modeled ore-bodies is also included; therefore, March's solution can be used to test the modeling system.

Let us refer to the spherical coordinate system of figure 10, where the center of the sphere is the coordinate

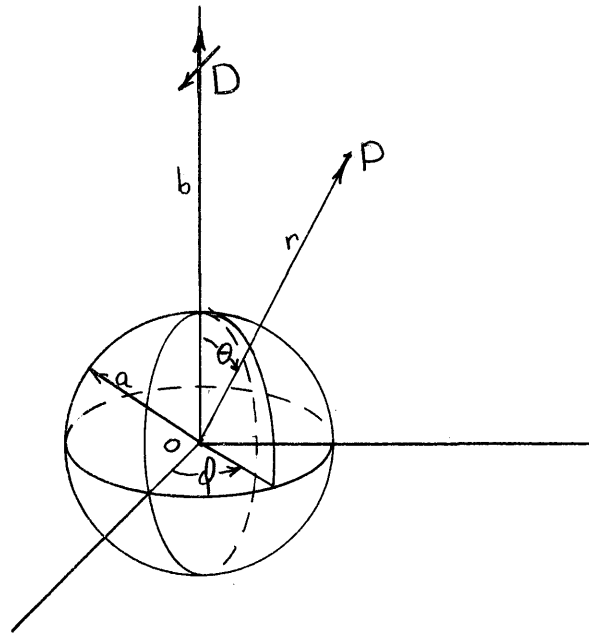


Figure 10 - Spherical coordinates of March's sphere solution

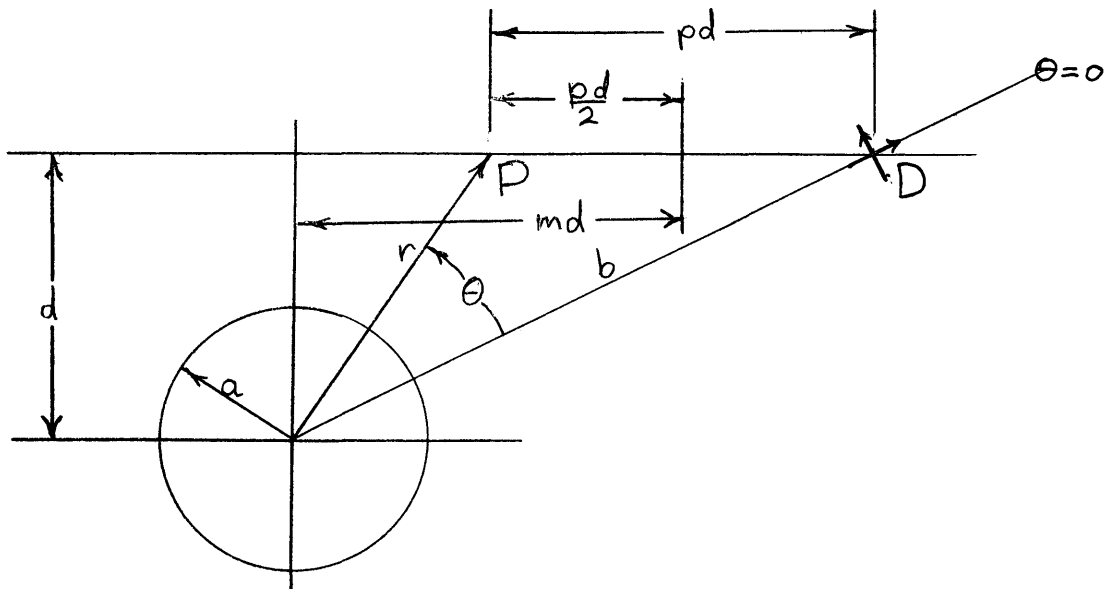


Figure 11 - Modeling dimensions and parameters in $d = 0$ plane of March's coordinate system

ϕ_2^a for the tangential dipole, and P_2^a , Θ_2^a , ϕ_2^a for the radial dipole, respectively, in March's notation, which was followed in Appendix 4.) Setting $\phi = 0$, we get

$$U_t = \sum_{n=1}^{\infty} n D_n \frac{a^{2n+1}}{(br)^{n+2}} P_n'(\mu) \quad (1)$$

$$\Theta_t = \sum_{n=1}^{\infty} \left(\frac{n}{n+1}\right) D_n \frac{a^{2n+1}}{(br)^{n+2}} (1-\mu^2)^{1/2} \frac{d}{d\mu} P_n'(\mu) \quad (2)$$

$$\phi_t = 0 \quad (3)$$

$$U_r = -\sum_{n=1}^{\infty} n(n+1) D_n \frac{a^{2n+1}}{(br)^{n+2}} P_n(\mu) \quad (4)$$

$$\Theta_r = -\sum_{n=1}^{\infty} n D_n \frac{a^{2n+1}}{(br)^{n+2}} P_n'(\mu) \quad (5)$$

$$\phi_r = 0 \quad (6)$$

where $\mu = \cos \theta$, $P_n(\mu)$ and $P_n'(\mu)$ are Legendre functions, and D_n is a complex function of conductivity σ , angular

frequency ω , and sphere radius a . Values of amplitude and complex phase angle for D_n for $n=1, 2$, and 3 are plotted by Robinson (1950, p. 28-29) as functions of σ, ω , and a .

The following transformations are derived directly from figure 11.

$$b = d \left[\left(m + \frac{p}{2} \right)^2 + 1 \right]^{1/2} \quad (7)$$

$$r = d \left[\left(m - \frac{p}{2} \right)^2 + 1 \right]^{1/2} \quad (8)$$

$$br = d^2 \gamma \quad (9)$$

$$\mu = \frac{1}{\gamma} \left[\left(m + \frac{p}{2} \right) \left(m - \frac{p}{2} \right) + 1 \right] \quad (10)$$

where

$$\gamma = \left\{ \left[\left(m - \frac{p}{2} \right)^2 + 1 \right] \left[\left(m + \frac{p}{2} \right)^2 + 1 \right] \right\}^{1/2} \quad (11)$$

Letting $c = \frac{a}{d}$ we get

$$\frac{a^{2n+1}}{(br)^{n+2}} = \frac{c^3}{d^3 \gamma^3} \left(\frac{c^2}{\gamma} \right)^{n-1} \quad (12)$$

Substituting (12) into equations (1), (2), (4) and (5), we get

$$U_t = \frac{c^3}{d^3 \gamma^3} \sum_{n=1}^{\infty} n \left(\frac{c^2}{\gamma} \right)^{n-1} D_n P_n'(\mu) = \frac{c^3}{d^3 \gamma^3} T_1 \quad (13)$$

$$\theta_t = \frac{c^3}{d^3 \gamma^3} \sum_{n=1}^{\infty} \binom{n}{n+1} \left(\frac{c^2}{\gamma} \right)^{n-1} D_n (1-\mu^2)^{1/2} \frac{d}{d\mu} P_n'(\mu) = -\frac{c^3}{d^3 \gamma^3} T_3 \quad (14)$$

$$U_r = -\frac{c^3}{d^3 \gamma^3} \sum_{n=1}^{\infty} n(n+1) \left(\frac{c^2}{\gamma} \right)^{n-1} D_n P_n(\mu) = -\frac{c^3}{d^3 \gamma^3} T_2 \quad (15)$$

$$\theta_r = -\frac{c^3}{d^3 \gamma^3} \sum_{n=1}^{\infty} n \left(\frac{c^2}{\gamma} \right)^{n-1} D_n P_n'(\mu) = -\frac{c^3}{d^3 \gamma^3} T_1 \quad (16)$$

where

$$T_1 = \sum_{n=1}^{\infty} n \left(\frac{c^2}{\gamma} \right)^{n-1} D_n P_n'(\mu) \quad (17)$$

$$T_2 = \sum_{n=1}^{\infty} n(n+1) \left(\frac{c^2}{\gamma} \right)^{n-1} D_n P_n(\mu) \quad (18)$$

$$T_3 = - \sum_{n=1}^{\infty} \binom{n}{n+1} \left(\frac{c^2}{\gamma}\right)^{n-1} D_n (1-\mu^2)^{\frac{1}{2}} \frac{d}{d\mu} P'_n(\mu) \quad (19)$$

For a unit vertical dipole at D the radial and transverse component dipoles are $\frac{d}{b}$ and $\frac{d}{b} (m + \frac{p}{2})$, respectively. Therefore the total secondary field at P is

$$H = \frac{c^3}{d^3 \gamma^3} \left[\underline{r}_1 \left\{ \frac{d}{b} \left(m + \frac{p}{2}\right) T_1 - \frac{d}{b} T_2 \right\} - \underline{\theta}_1 \left\{ \frac{d}{b} \left(m + \frac{p}{2}\right) T_3 + \frac{d}{b} T_1 \right\} \right] \quad (20)$$

where \underline{r}_1 and $\underline{\theta}_1$ are unit vectors. Because the receiving coil is horizontal, it senses only the vertical component of the secondary field.

$$H_v = \frac{c^3}{d^3 \gamma^4} \left\{ p T_1 - T_2 - \left(m + \frac{p}{2}\right) \left(m - \frac{p}{2}\right) T_3 \right\} \quad (21)$$

To express this as a fraction Z of the primary field, divide H_v by $H_p = -\frac{1}{(pd)^3}$, the vertical component of the primary field at P due to a unit vertical dipole at D.

$$Z = \frac{H_v}{H_p} = \frac{c^3 p^3}{\gamma^4} \left\{ -p T_1 + T_2 + \left(m + \frac{p}{2}\right) \left(m - \frac{p}{2}\right) T_3 \right\} \quad (22)$$

It is significant to note from equations (1) through (6) that b and r, the radial distances to the source and receiver respectively, can be interchanged without

altering the equations. This fact holds throughout the subsequent development and implies reciprocity. Thus the in-phase and quadrature curves from running a traverse over a sphere should be symmetric about the $m=0$ position.

Experimental data were taken at $d = 0.500$ ft and 0.333 ft over a 500 ml mercury sphere contained in a spherical glass flask. The mercury was clean but not redistilled. The coil separation, pd , was 1.000 ft in both cases. The resulting in-phase and quadrature curves are shown in figures 12 and 13. Theoretical values for the position $m=0$, $p=2$ are more readily calculated than for any other position. Based on the conductivity of pure mercury ($\sigma = 1.04 \times 10^6$ mhos/m at 23°C) the theoretical anomaly at $m=0$, $p=2$, was calculated to be

$$Z = -0.0146 - i 0.0115$$

whereas the corresponding experimental anomaly was

$$Z_e = -0.0191 - i 0.0113.$$

These discrepancies of +31% and -1.4% from the theoretical in-phase and quadrature values may be due to impurities in the mercury which increase its conductivity. However, from the limited data appearing in the Handbook of Chemistry and Physics about amalgams, it seems that impurities generally tend to decrease the conductivity of mercury.

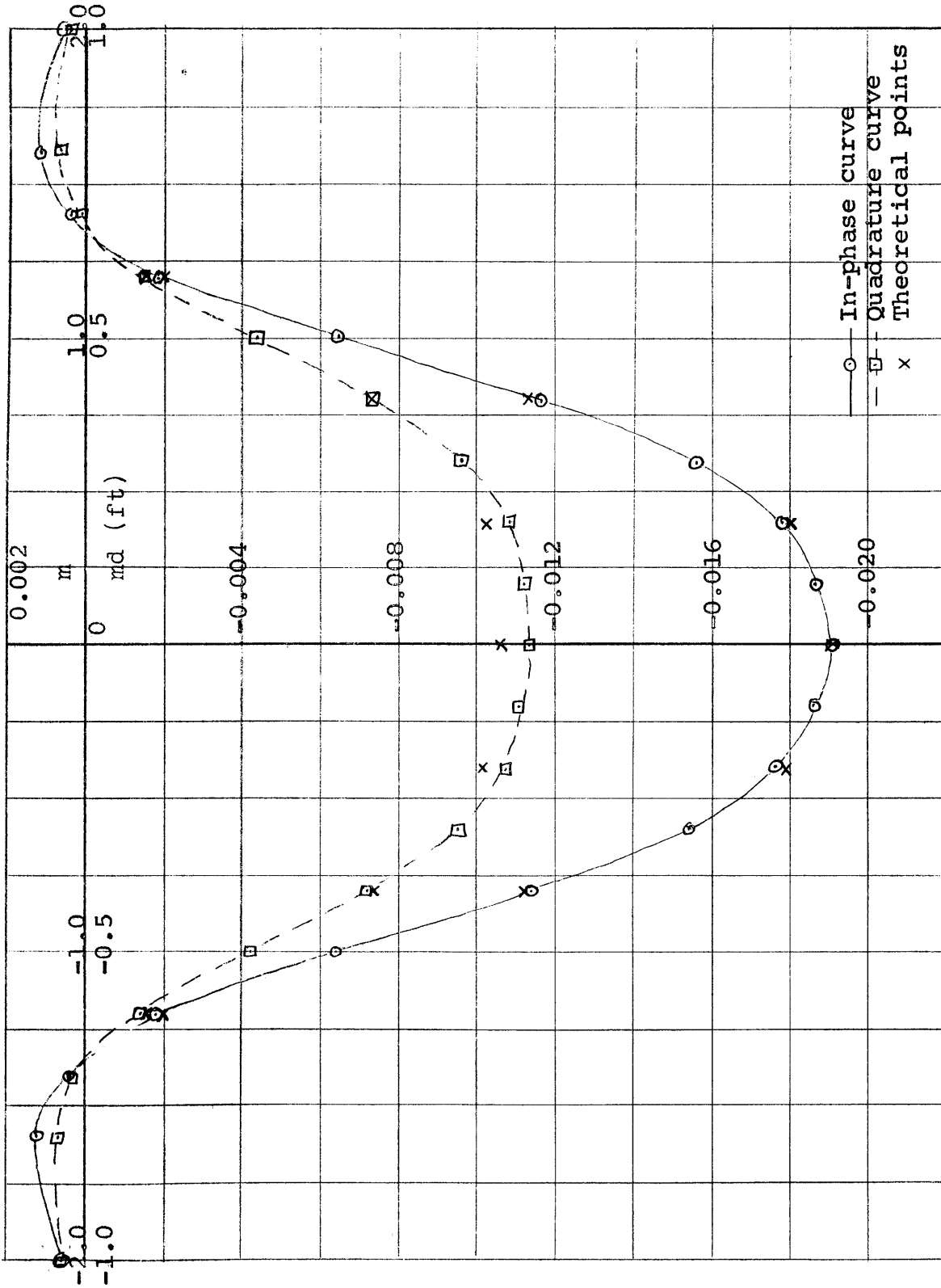


Figure 12 - Experimental and theoretical anomalies over 500 ml mercury sphere - $d = 0.500$ ft, $a = 0.1615$ ft, $p = 2.000$
 $\sigma = 1.6 \times 10^6$ mhos/m

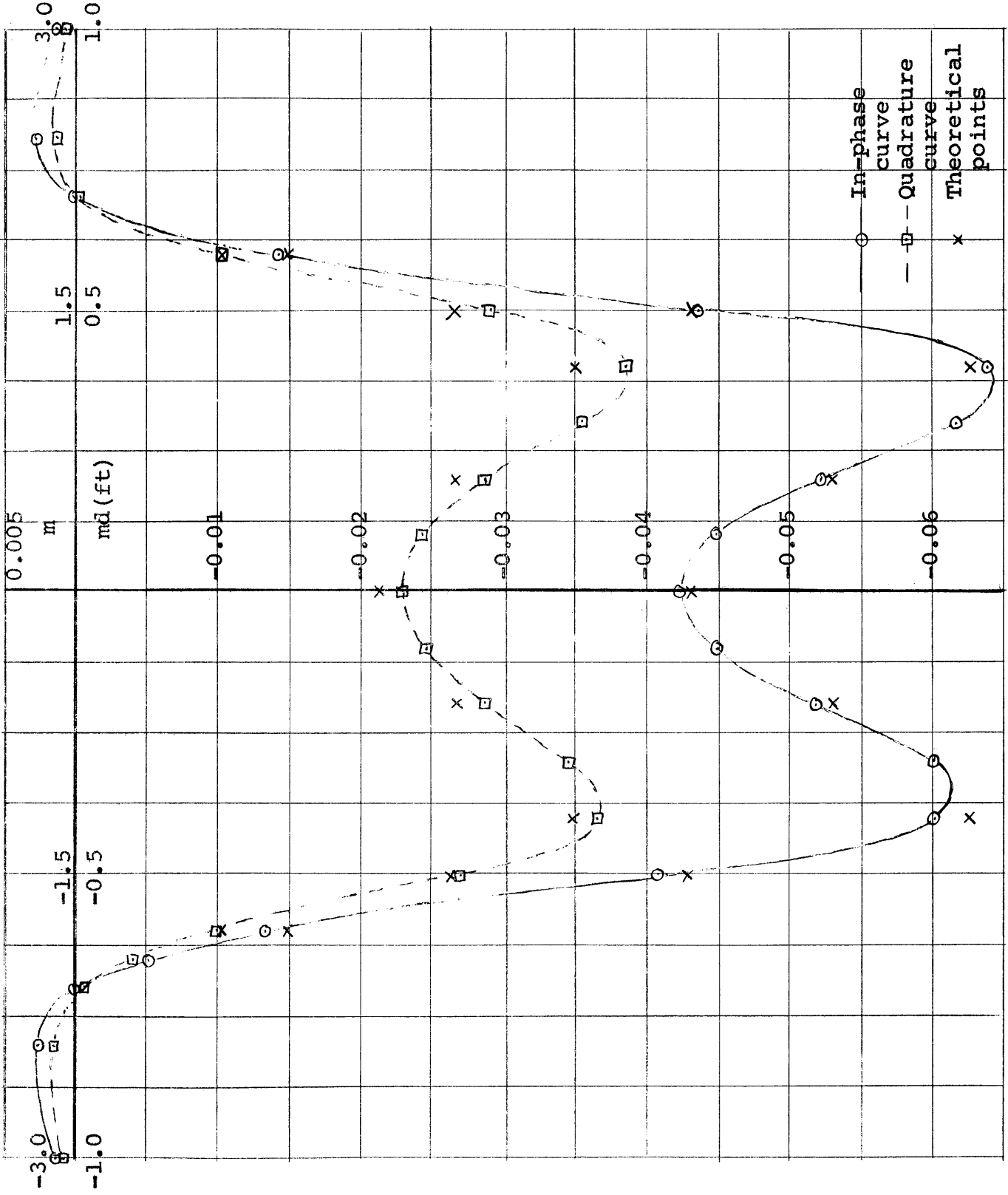


Figure 13 - Experimental and theoretical anomalies over 500 ml mercury sphere - $d = 0.333$ ft, $a = 0.1615$ ft, $p = 3.000$
 $G = 1.6 \times 10^6$ mhos/m

Nevertheless, it may be noted that a conductivity of $\sigma = 1.6 \times 10^6$ mhos/m yielded a theoretical anomaly of

$$Z = -0.0191 - i 0.0105$$

at $m=0$, $p=2$, with the experimental in-phase and quadrature values differing by 0% and 7.6% respectively. Although their agreement is relatively good, its significance should be tested by measuring the conductivity of the mercury used, or by rerunning traverses over a sphere of pure mercury or other sphere of known conductivity. If such tests continued to yield discrepancies between theoretical and experimental results, it might well be necessary to re-examine the limitations of March's solution. (It is interesting to note that Robinson, too, had to use an assumed value of conductivity for his aluminum spheres in order to obtain agreement between experimental measurements and theoretical results based on March's solution.)

Using the higher value of conductivity, several theoretical values were calculated for each experimental curve and are superimposed on figures 12 and 13. The agreement is good, particularly for the case where $d = 0.500$ ft. The slight asymmetry of figure 13 may be caused by one or more of the following factors:

- 1) Quadrupole and higher multipole fields in the vicinity of the source coil.

- 2) Imperfect sphericity of the mercury, particularly on top.
- 3) Effect of secondary field on the reference-coil signal.

Further investigations might well be conducted to determine which of the above factors, or other possible factors, are the principle causes of asymmetry.

CONCLUSIONS

This section deals with several practical aspects of the instrumentation problem of this thesis which are worthy of consideration. Following are brief discussions of alternative approaches, significant observations, and suggested improvements.

Alternative Approaches

There are several approaches to measuring the secondary field which might work just as well as or better than the method developed in this thesis. In the three alternatives examined below only the components corresponding to the a-c comparator are discussed. A reference circuit to provide the comparator with a properly phase-shifted and attenuated reference signal is assumed to be available.

If one wished to measure magnitude and phase angle of the secondary field rather than the quadrature components, a simpler circuit could be designed to buck out the receiver signal. One such circuit with its corresponding phase diagram is suggested in figure 14.

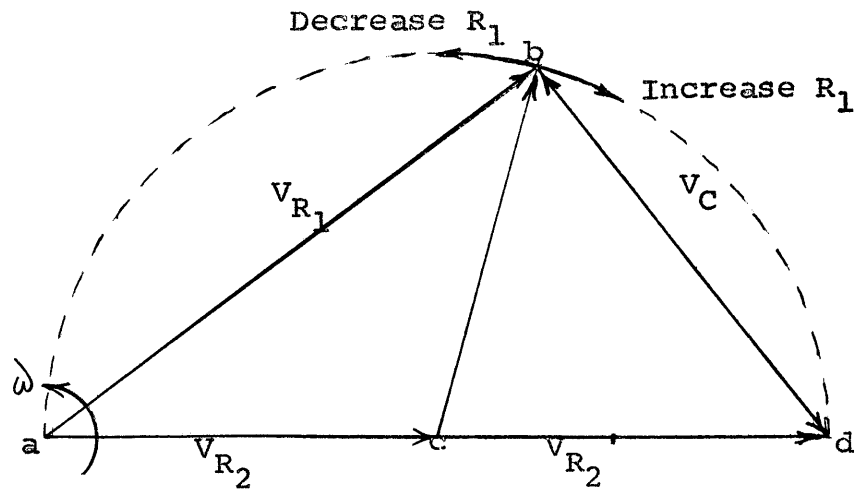
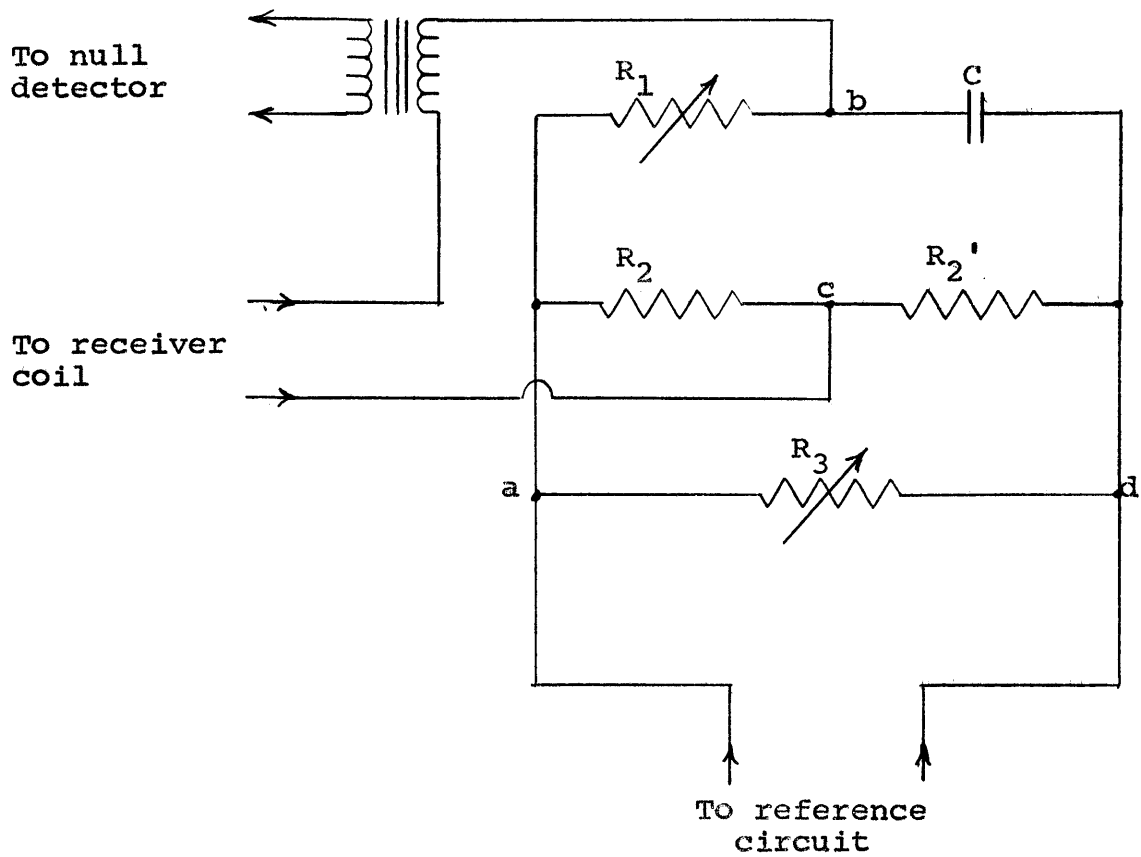


Figure 14 - Circuit and phase diagrams for measuring magnitude and phase of secondary field

If R_1 and X_c are much larger than the combined resistance of R_2 , R_2' , and R_3 across a-c, then R_1 controls signal phase without affecting magnitude and R_3 controls magnitude without affecting phase. The advantages of such a circuit are its simplicity and its requirement of only one pair of matched components. A disadvantage is that R_1 and R_3 must have specially calibrated dials to read phase and magnitude directly. Also, if results are to be plotted in terms of in-phase and quadrature components, data reduction would require an appreciable amount of time.

An interesting approach to measuring in-phase and quadrature components directly is used in Ronka field instruments and might well be the basis of a modeling system. This method requires a reference signal much larger than the receiver signal. The circuit and corresponding phase diagram are suggested in figure 15. If $V_{C1} \gg V_{R2}$, then V_{R2} is essentially at quadrature with V_{R4} . R_4 and R_1 are then the in-phase and quadrature potentiometers. This comparator circuit has the advantage of being slightly simpler than the circuit developed in this thesis. However, it requires a much larger reference signal. For reasons to be mentioned later, this signal must be provided by a coil wound on or near the source-coil rather than directly by the power amplifier. In view of the large size of the

source-coil used in the modeling instrumentation, an additional large coil in the source vicinity was thought to be undesirable because of secondary effects. However, in retrospect I believe that the high sensitivity of the null-detecting system would permit using a much smaller source-coil and a somewhat larger reference-coil than were actually used, thus fulfilling the requirements for the Ronka approach. Such a system might well prove to be simpler in design and as good in performance as the system used.

A third approach uses a comparator circuit similar to the one actually used or the one described above. But instead of adding the receiver signal to the comparator signal through a resistive and capacitive coupling circuit, the signals are added by a purely inductive coupling, achieved as shown in figure 16. The signal produced by the comparator circuit drives the high-impedance input of a cathode-follower stage. The high-impedance input is necessary to avoid loading the comparator circuit. The cathode-follower output must be proportional in magnitude to its input and must have a constant phase relationship with its input over the operating range. The low-impedance output drives a bucking-coil which is wound on or near the receiver-coil. The null-detector is coupled directly

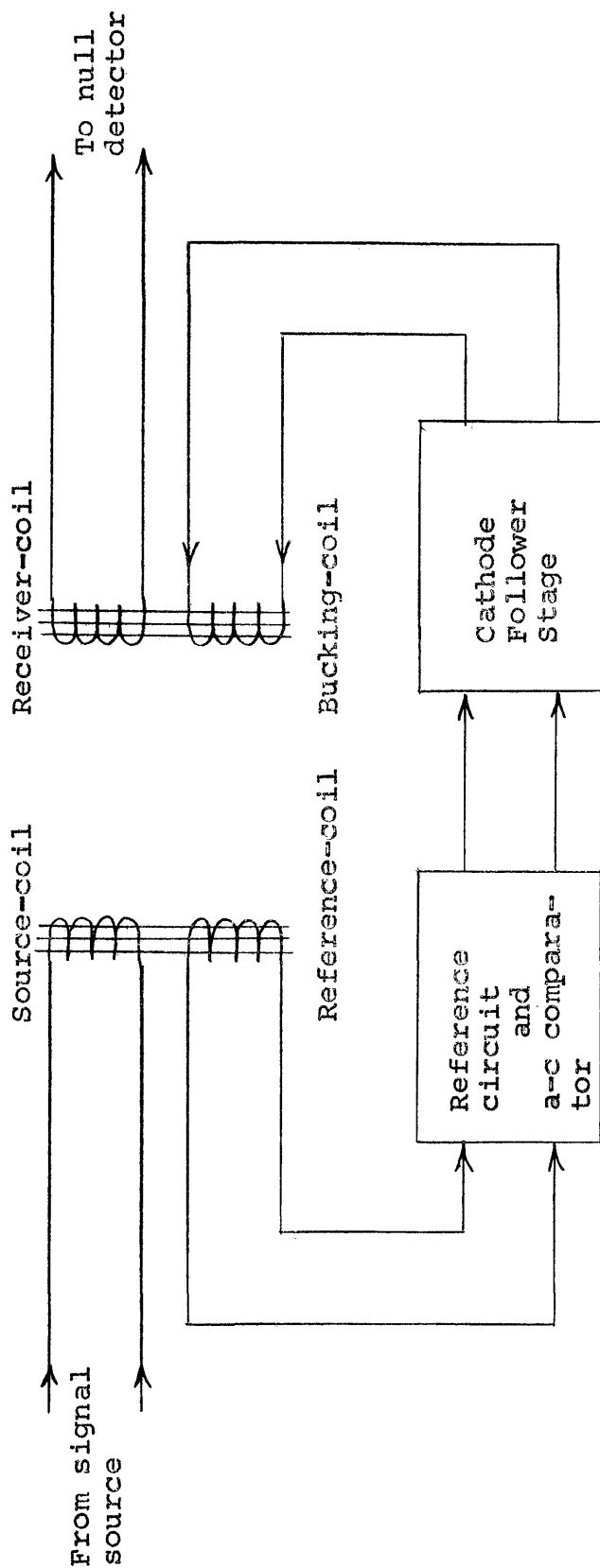


Figure 16 - Circuit diagram for "bucking coil" method of measuring in-phase and quadrature components of secondary field

to the receiver-coil. When the comparator parameters are adjusted so that the field of the bucking-coil exactly cancels the primary and secondary fields at the receiver-coil, a null is achieved. The field from the bucking-coil is much weaker than the source field and will therefore cause no appreciable secondary field of its own. This method is used in at least one make of field equipment. Because the receiver signal is cancelled by a purely inductive coupling, this alternative has the advantage of not requiring balanced circuits and coils, or elaborate shielding. This advantage may be far more valuable in field equipment than under controlled laboratory conditions. Nevertheless, it is worth consideration as the basis for a modeling system.

Significant Observations

While building up the modeling system for this thesis, several observations were made which might be of value in future work of this sort.

Transformers to isolate circuit components should be avoided wherever possible. Unless they are high-quality transformers with shielded windings, there may well be enough capacitive coupling between the primary and secondary windings to cause appreciable unbalancing of an otherwise

balanced circuit, such as the a-c comparator. The only transformer in the final comparator circuit was used to isolate the output to the null-detector. It is a high-quality audio transformer, designed for broadcast-line service, and has shielded windings.

Balancing the comparator circuit to achieve equal voltages at all symmetric points requires painstaking care in matching components because slight mismatching seems to have a cumulative effect in unbalancing the voltage across the quadrature potentiometer. It is good practice to build the circuit into the chassis with as much physical symmetry as possible in order to balance stray capacitances to ground. It is of equal importance that the reference signal be carefully balanced. The final reference-coil used was center-tapped and grounded to the shield of the two-conductor cable bringing the reference signal to the comparator. The shield was in turn grounded to the comparator chassis which was connected directly to the building frame. The physical location of the reference-coil center-tap was adjusted until a balanced signal was obtained at the comparator.

At one time during the system development, the reference signal was taken directly from the balanced output of the power amplifier. As a result of getting

highly asymmetric anomaly curves from traversing over the mercury sphere, it was discovered that the phase between the current in the source-coil and the output voltage of the power amplifier was not constant throughout the traverse. When the tuned high-Q source-coil was near the mercury, its self-inductance and equivalent-resistance changed enough to introduce a phase shift. The solution was to take the reference signal from a source which follows the primary field, i.e., the source-coil circuit. The coil wound directly on the source-coil and described in the previous paragraph provided the necessary signal.

Suggested Improvements

Following are several ideas for improving the present modeling system.

The major area for improvement is in the coils. The null-detector system is sensitive enough, and background noise low enough, that significantly smaller source- and receiver-coils could be used. This would reduce higher multipole fields in the vicinity of the source-coil, and decrease the area over which the receiver-coil measures an average field strength. Both of these improvements might tend to reduce the asymmetry, and other deviations from theory, noted earlier in connection with

the sphere anomaly curves. I would predict that coils with a 3/4-in. outside diameter, 1/2-in. hole diameter, and 1/4-in. height would work well.

Because of the large voltage across the tuned source-coil, it would be advisable to put a grounded shield between the source- and reference-coils to reduce capacitive coupling. At the same time the reference-coil should be wound directly on the source-coil to have maximum inductive coupling with the source. This close coupling minimizes the relative effect of the secondary field on the reference signal.

The source- and reference-coils should be wound in two symmetric parts in order to balance capacitive effects with the surroundings and with each other. The receiver voltage "floats" relative to the grounded center-tap of the bridge, and therefore need not be balance-wound.

As noted earlier, the symmetry of sphere anomaly curves might be improved by eliminating the possibility of the secondary field having an effect on the reference-coil signal. This could be accomplished by taking the reference signal from the feed line to the source-coil by means of a transformer far removed from the source-coil. Such an arrangement would also eliminate the possibility of the reference-coil current affecting the primary field.

APPENDICES

The four appendices of this section deal with the following subjects:

- 1) Preparation for Taking Data
- 2) Taking and Reducing Data
- 3) A-C Comparator Calibration
- 4) Extension of March's Sphere Solution for the Case of Finite Sphere Conductivity

Appendix 1 - Preparation for Taking Data

Following is a step-by-step procedure for preparing to take data:

1. The power amplifier input circuit is adjusted to zero signal (attenuation knob counterclockwise).
2. The voltage regulator, fork oscillator, power amplifier, and narrow-band amplifier power supply (300-v switch off) are turned on to warm up.
3. The coil carriage is brought to the 0.000 ft position and the coil height and horizontal angle and the model ore-body are adjusted to the desired

orientation. A scale and plumb bob may be useful.

4. The coil carriage is slid to a position remote from the ore model, such as -5 ft.
5. The power amplifier input signal is adjusted for 20-v across the source-coil circuit.
6. The preamplifier, decade amplifier (10x), and 300-v switch of the narrow-band amplifier power supply are turned on. The plate voltage is adjusted to 300-v. The narrow-band amplifier feedback control knob is turned to point to the left.
7. The in-phase and quadrature dials are set to read 5.000.
8. The operator puts the earphones on and successively adjusts the two reference circuit controls ($R_8 - R_8'$ and R_7') to get a null. It may be temporarily necessary to set the dials to positions other than 5.000 in order to determine which way to turn the reference signal controls.
9. If step 8 requires changing the upper reference control ($R_8 - R_8'$) by more than a small fraction of a turn, the chassis is opened and V_i and V_i are measured. If they are not equal, R_{10} is

adjusted until they are equal. This adjustment is necessary since R_g and R_g' do not have identical characteristics. The chassis is closed and step 8 is repeated.

10. The decade amplifier is switched to 100x and the narrow-band amplifier feedback is increased to just below oscillation in order to increase the gain and narrow the band-width so as to achieve maximum null sensitivity.
11. If necessary, step 8 is repeated so that null occurs with dials as nearly at 5.000 as possible. The primary signal from the receiver is now canceled out. The dial readings are recorded and the traverse can now be run.

Appendix 2 - Taking and Reducing Data

1. The coil carriage is moved to the first position in the traverse.
2. The two potentiometer dials are successively adjusted so as to achieve a null, and the dial readings are recorded.
3. The coil carriage is moved to the next position in the traverse and step 2 is repeated.
4. Step 3 is repeated until the traverse is completed. The carriage is returned to the position remote from the model, the comparator is adjusted for a null, and the dial readings are recorded. These readings should be essentially identical to the readings of step 11 of the previous paragraph.

The equations for reducing dial readings to in-phase and quadrature percentages are readily found from examination of the comparator phase and circuit diagrams. Let E_r be the in-phase dial reading at the remote position and E_t be the reading at some position along the traverse. Let E_r' and E_t' be the corresponding quadrature dial readings. Then

$$\text{in-phase percent} = 20 (E_r - E_t)$$

$$\text{quadrature percent} = 10 (E_t' - E_r').$$

Appendix 3 - A-C Comparator Calibration

In order for the in-phase and quadrature potentiometers to give correct measurements of the secondary field, the a-c comparator must be adjusted to correspond to the phase diagram of figure 5. The necessary instruments are a high-impedance millivoltmeter and a 1000-cps signal source. In reference to both the phase diagram and the circuit diagram of figure 5, the adjustment procedure is as follows:

1. A balanced 1000-cps signal is connected across g-k. The usual reference signal can be used.
2. With i grounded, V_{ig} is measured.
3. R_5' is adjusted so that $V_{ip} = (1/4)V_{ig}$. The extreme settings of the quadrature potentiometer, R_4 , now correspond to +50% and -50% of the primary field signal.
4. The signal source is reconnected across g-k so that g is grounded instead of i.
5. R_6' is adjusted so that $V_{gp} = V_{gq}$. The voltages across the two potentiometers are now at quadrature.
6. Steps 1 to 5 are repeated until conditions 3 and 5 are satisfied simultaneously.

The above adjustments should not have to be made again unless the operating frequency is changed or the value of some circuit component is altered. If the input signal is balanced and i is grounded, symmetric points in the circuit should always have identical voltages with respect to ground. One or more pairs of poorly matched components would cause an unbalance. Also, if the voltages are balanced, V_{ie} should be a minimum when the quadrature potentiometer is set on 5.000.

Appendix 4 - Extension of March's Sphere Solution for the
Case of Finite Sphere Conductivity

The following development assumes that the reader has reviewed March's solution (1953) for the field of a magnetic dipole in the presence of a conducting sphere, and that he has the article available. March's notation is used below.

The magnetic field components arising from the first partial secondary field of the transverse magnetic dipole can be neglected when compared to the second partial secondary field components since they contain the factor k_a^2 , where $k_a \ll 1$. The first step in March's solution which renders the subsequent development of the components of the second partial secondary field insufficiently accurate for the model work is March's equation (74) where he sets $\lim_{\sigma_i \rightarrow \infty} D_n = 1$. Immediately prior to this step the potential function giving rise to the second partial field is given by March's equation (72),

$$\pi_2^a = \left(\frac{i \cos \phi}{br} \right) \sum_{n=1}^{\infty} \left[\frac{2n+1}{n(n+1)} \right] D_n \left[\frac{\zeta_n'(k_a a)}{\xi_n(k_a a)} \right] \xi_n'(k_a b) \xi_n(k_a r) P_n'(\cos \theta) \quad (1)$$

where values of D_n for finite sphere conductivity are plotted by Robinson (1950). For small values of $x = k_a a$, the formulas for $\zeta_n'(x)$, $\zeta_n(x)$, $\xi_n(x)$ and $\xi_n'(x)$

given in March's equations (63) can be substituted into (1) yielding

$$\Pi_2^a = \cos \phi \sum_{n=1}^{\infty} \left(\frac{1}{n+1} \right) \left(\frac{a^{2n+1}}{b^{n+2} r^{n+1}} \right) D_n P_n'(\cos \theta) \quad (2)$$

Using this form for Π_2^a , the components P_2^a , Θ_2^a , and Φ_2^a can be derived from March's equations (9).

$$P_2^a = \frac{\partial^2 (r \Pi_2^a)}{\partial r^2} + k^2 r \Pi_2^a = \cos \phi \sum_{n=1}^{\infty} n D_n \frac{a^{2n+1}}{(br)^{n+2}} P_n'(\cos \theta) \quad (3)$$

$$\Theta_2^a = \frac{1}{r} \frac{\partial^2 (r \Pi_2^a)}{\partial r \partial \theta} = \cos \phi \sin \theta \sum_{n=1}^{\infty} \left(\frac{n}{n+1} \right) D_n \frac{a^{2n+1}}{(br)^{n+2}} \frac{\partial P_n'(\cos \theta)}{\partial (\cos \theta)} \quad (4)$$

$$\Phi_2^a = \frac{1}{r \sin \theta} \frac{\partial^2 (r \Pi_2^a)}{\partial r \partial \phi} = \sin \phi \sum_{n=1}^{\infty} \left(\frac{n}{n+1} \right) D_n \frac{a^{2n+1}}{(br)^{n+2}} \frac{P_n'(\cos \theta)}{\sin \theta} \quad (5)$$

The components of the secondary field arising from the radial dipole are obtained entirely from Π_2^a for the radial dipole since $\Pi_1^a = 0$. From March's equation (82),

$$\Pi_2^a = \left(\frac{i}{k_a b^2 r} \right) \sum_{n=0}^{\infty} (2n+1) D_n \left[\frac{z_n^2(k_a a)}{\xi_n(k_a a)} \right] \xi_n(k_a b) \xi_n(k_a r) P_n(\cos \theta) \quad (6)$$

Again substitute the approximations of March's equation (63) into (6) to derive

$$\Pi_2^a = - \sum_{n=0}^{\infty} D_n \frac{a^{2n+1}}{b^{n+2} r^{n+1}} P_n(\cos \theta) \quad (7)$$

Substituting (7) into March's equations (9) one can derive

$$P_2^a = - \sum_{n=1}^{\infty} n(n+1) D_n \frac{a^{2n+1}}{(br)^{n+2}} P_n(\cos \theta) \quad (8)$$

$$\Theta_2^a = - \sum_{n=1}^{\infty} n D_n \frac{a^{2n+1}}{(br)^{n+2}} P_n'(\cos \theta) \quad (9)$$

$$\Phi_2^a = 0 \quad (10)$$

for the radial dipole. These components together with the corresponding components arising from the transverse dipole, constitute the desired solution for the field of a magnetic dipole in the presence of a sphere of finite conductivity.

SELECTED BIBLIOGRAPHY

1. Clark, A. R. and Mungal, A.G., 1951, Scale model experiments in electromagnetic methods of geophysical exploration: Canadian Jour. of Phys., v. 29, no. 4, p. 285-295.
2. Edwards, M. A., 1956, The instrumentation of small scale modelling for airborne electromagnetic surveying: Univ. of Western Ontario, Master's Thesis, 43 p.
3. Forbes, R. F. S., 1957, Modeling of the electromagnetic response of mineral bodies as a function of conductivity: Univ. of Calif. at Los Angeles, Doctoral Thesis, 84 p.
4. Frischknecht, F. C., 1959, Scandinavian electromagnetic prospecting: Mining Eng., v. 11, no. 9, p. 932-937.
5. Hedström, E. H., 1937, Phase measurement in electrical prospecting: Am. Inst. Mining Metall. Petroleum Engineers Tech. Pub. no. 827, p. 16-17.
6. Hedström, E. H., and Parasnis, D. S., 1958, Some model experiments relating to electromagnetic prospecting with special reference to airborne work: Geophys. Prosp., v. VI, no. 4, p. 322-341.
7. Hund, A., 1936, Phenomena in high-frequency systems: New York, McGraw Hill, 642 p.
8. _____ 1951, High frequency measurement: New York, McGraw Hill, 676 p.
9. Jakosky, J. J., 1940, Exploration geophysics: Newport Beach, Calif., Trija Publishing Company, p. 581-638.
10. March, H. W., 1953, The field of a magnetic dipole in the presence of a conducting sphere: Geophysics, v. XVIII, no. 3, p. 671-684.

11. Panofsky, W. K. H., and Phillips, M., 1955, Classical electricity and magnetism: Reading, Mass., Addison-Wesley, 392 p.
12. Patkau, B. H., 1953, A test of the response of cylindrical conductors to electromagnetic induction by model experiments: Univ. of Toronto, Master's Thesis, 43 p.
13. Robinson, W. J., 1950, Observed and theoretical electromagnetic response of conducting spheres: Univ. of Toronto, Master's Thesis, 48 p.
14. Rogers, G. R., 1957, Electromagnetic prospecting methods: Mines Mag. [Colorado], v. 47, no. 12, p. 26-30.
15. Sinclair, G., 1948, Theory of models of electromagnetic systems: IRE Proc., v. 36, no. 11, p. 1364-1370.
16. Smythe, W. R., 1950, Static and dynamic electricity: New York, McGraw Hill, 616 p.
17. Stratton, A. S., 1941, Electromagnetic theory: New York, McGraw Hill, p. 488-490.
18. Tesche, F. R., 1951, Instrumentation of electromagnetic modeling, and application to electromagnetic prospecting: Univ. of Calif., Doctoral Thesis, 81 p.
19. Wait, J. R., 1951, Conducting sphere in a time varying magnetic field: Geophysics, v. XVI, no. 4, p. 666-672.
20. _____ 1953, A conducting permeable sphere in the presence of a coil carrying an oscillating current: Canadian Jour. Phys., v. 31, no. 3, p. 670-679.
21. Ward, S. H., 1950, Model testing - an approach to the problem of interpretation in the electromagnetic method of geophysical prospecting: Univ. of Toronto, Master's Thesis, 28 p.
22. _____ 1952, A theoretical and experimental study of the electromagnetic method of geophysical prospecting: Univ. of Toronto, Doctoral Thesis, 108 p.
23. _____ 1959, Unique determination of conductivity, susceptibility, size and depth in multifrequency

- electromagnetic exploration: *Geophysics*, v. XXIV, no. 3, p. 531-546.
24. _____ 1959, AFMAG - airborne and ground: *Geophysics*, v. XXIV, no. 4, p. 761-789.
25. Waters, G. S., and Francis, P. D., 1958, A nuclear magnetometer: *Jour. of Sci. Instruments*, v. 35, p. 91.
26. Wesley, J. P., 1958, Response of dyke to oscillating dipole: *Geophysics*, v. XXIII, no. 1, p. 128-133.
27. _____ 1958, Response of thin dyke to oscillating dipole: *Geophysics*, v. XXIII, no. 1, p. 134-143.
28. West, G. F., 1957, Theoretical studies for induction prospecting: Univ. of Toronto, Master's Thesis, 35 p.
29. _____ 1960, Quantitative interpretation of electromagnetic prospecting measurements: Univ. of Toronto, Doctoral Thesis, 163 p.